2014

Multi-leg one-loop massive amplitudes from integrand reduction via Laurent expansion

Hans van Deurzen
Max-Planck Insitut fur Physik

Gionata Luisoni
Max-Planck Insitut fur Physik

Pierpaolo Mastrolia
Max-Planck Insitut fur Physik

Edoardo Mirabella
Max-Planck Insitut fur Physik

Giovanni Ossola
CUNY New York City College of Technology

See next page for additional authors

Authors

Hans van Deurzen, Gionata Luisoni, Pierpaolo Mastrolia, Edoardo Mirabella, Giovanni Ossola, and Tiziano Peraro

Multi-leg one-loop massive amplitudes from integrand reduction via Laurent expansion

Hans van Deurzen,[a] **Gionata Luisoni,**[a] **Pierpaolo Mastrolia,**[a,b] **Edoardo Mirabella,**[a] **Giovanni Ossola**[c,d] **and Tiziano Peraro**[a]

[a]*Max-Planck Insitut für Physik,*
Föhringer Ring, 6, D-80805 München, Germany

[b]*Dipartimento di Fisica e Astronomia, Università di Padova, and INFN Sezione di Padova,*
via Marzolo 8, 35131 Padova, Italy

[c]*Physics Department, New York City College of Technology, The City University of New York,*
300 Jay Street Brooklyn, NY 11201, U.S.A.

[d]*The Graduate School and University Center, The City University of New York,*
365 Fifth Avenue, New York, NY 10016, U.S.A.

E-mail: hdeurzen@mpp.mpg.de, luisonig@mpp.mpg.de,
pierpaolo.mastrolia@cern.ch, mirabell@mpp.mpg.de,
GOssola@citytech.cuny.edu, peraro@mpp.mpg.de

ABSTRACT: We present the application of a novel reduction technique for one-loop scattering amplitudes based on the combination of the integrand reduction and Laurent expansion. We describe the general features of its implementation in the computer code NINJA, and its interface to GOSAM. We apply the new reduction to a series of selected processes involving massive particles, from six to eight legs.

Contents

1 Introduction

Scattering amplitudes in quantum field theories are analytic functions of the kinematic variables of the interacting particles, hence they can be determined by studying the structure of their singularities.

The multi-particle factorization properties of the amplitudes become transparent when internal particles go on their mass-shell [1, 2]. These configurations correspond to poles of the amplitude and the investigation of the general structure of the residues corresponding to multi-particle factorization channel turns out to be of particular interest. Indeed the knowledge of such structure has been fundamental for discovering new relations fulfilled by scattering amplitudes, such as the BCFW recurrence relation [3] and its link to the leading singularity of one-loop amplitudes [4]. The systematic classification of the residues, for all the poles corresponding to the quadruple, triple, double, and single cuts, has been achieved, in four dimensions, by employing integrand-reduction methods [5, 6]. The latter led to the OPP integrand-decomposition formula for one-loop integrals [6], which allows one to write each residue as a linear combination of process-independent polynomials multiplied by process-dependent coefficients.

These results provided a deeper understanding of the structure of scattering amplitudes and have shown the underlying simplicity beneath the rich mathematical structure of quantum field theory. Moreover, they provided the theoretical framework for the development of efficient computational algorithms for one-loop calculations in perturbation theory, which have been implemented in various automated codes [7–16] improving the state-of-the art of the predictions at the next-to-leading order accuracy [17–50].

Recently, the classification of the structure of the residues has been obtained in a more general and elegant form within the framework of multivariate polynomial division and algebraic geometry [51, 52]. The use of these techniques proved that the integrand decomposition, originally formulated for one-loop amplitudes, is applicable at any order in perturbation theory, irrespective of the complexity of the topology of the diagrams involved. An iterative integrand-recursion formula, based on successive divisions of the numerators modulo the Gröbner basis of the ideals generated by the cut denominators, can provide the form of the residues at all multi-particle poles for arbitrary amplitudes, independently of the number of loops. Extensions of the integrand reduction method beyond one-loop, initiated in [53, 54] and then systematized within the language of algebraic geometry [51, 52] have recently become the topic of several studies [55–60], thus providing a new direction in the study of multi-loop amplitudes.

In the context of the integrand reduction, the process-dependent coefficients can be numerically determined by solving a system of algebraic equations that are obtained by evaluating the numerator of the integrand at explicit values of the loop momentum [6]. The system becomes triangular if one evaluates the numerator at the multiple cuts, i.e. at the set of complex values of the integration momentum for which a given set of propagators vanish. The extraction of all coefficients via polynomial fitting has been implemented in publicly available codes performing integrand decomposition, such as CUTTOOLS [61] and SAMURAI [62]. These algorithms do not requires any specific recipe for the generation of

the numerator function, which can be performed by using traditional Feynman diagrams, by means of recursive relations, or by gluing tree-level sub-amplitudes, as in unitarity-based methods.

The code CUTTOOLS implements the four-dimensional integrand-reduction algorithm [63–65], in which the cut-constructible term and the rational term are necessarily computed separately. The latter escapes four-dimensional integrand reduction and has to be computed using other methods, e.g. by using *ad hoc* tree-level Feynman rules [65–72].

Significant improvements were achieved with the *d*-dimensional extension of integrand-reduction methods [73–75], which expose a richer polynomial structure of the integrand and allows for the combined determination of both cut-constructible and rational terms at once. This idea of performing unitarity-cuts in *d*-dimension was the basis for the development of SAMURAI, which extends the OPP polynomial structures to include an explicit dependence on the $(d-4)$-dimensional parameter needed for the automated computation of the full rational term. Moreover, it includes the parametrization of the residue of the quintuple-cut [76] and implements the numerical sampling via Discrete Fourier Transform [64].

The integrand decomposition was originally developed for renormalizable gauge theories, where, at one-loop, the rank of the numerator cannot be larger than the number of external legs. The reduction of diagrams where the rank can be higher, as required for example when computing $pp \to H + 2, 3$ jets in gluon fusion in the large top-mass limit [42, 44], demands an extension of the algorithm to accommodate the richer monomial structures of the residues. This extension has been implemented in SAMURAI, together with the corresponding sampling required to fit all the coefficients [77–79].

More recently, elaborating on the the techniques proposed in [80, 81], a different approach to the *d*-dimensional integrand-reduction method was proposed [78]. The key point of this method is to extract the coefficients more efficiently by performing a Laurent expansion of the integrand. The method is general and relies only on the knowledge of the explicit dependence of the numerator on the loop momentum.

In general, when the multiple-cut conditions do not fully constrain the loop momentum, the solutions are still functions of some free parameters, possibly the components of the momentum which are not frozen by the cut conditions. The integrand-reduction algorithms implemented in the codes [61, 62] require to solve a system of equations obtained by sampling on those free parameters. The system is triangular thus the coefficients of a given residue can be computed only after subtracting all the non-vanishing contributions coming from higher-point residues.

The key observation suggested in ref. [78] is that the reduction algorithm can be simplified by exploiting the universal structure of the residues, hence of their asymptotic expansion. Indeed, by performing a *Laurent expansion* with respect to one of the free parameters which appear in the solutions of the cut, both the integrand and the subtraction terms exhibit the same polynomial behavior of the residue. Moreover, the contributions coming from the subtracted terms can be implemented as *corrections at the coefficient level*, hence replacing the subtractions at the integrand level of the original algorithm. The parametric form of these corrections can be computed once and for all, in terms of a subset of the higher-point coefficients. This method significantly reduces the number

of coefficients entering each subtracted term, in particular boxes and pentagons decouple from the computation of lower-points coefficients.

If either the analytic expression of the integrand or the tensor structure of the numerator is known, this procedure can be implemented in a semi-numerical algorithm. Indeed, the coefficients of the Laurent expansion of a rational function can be computed, either analytically or numerically, by performing a *polynomial division* between the numerator and the (uncut) denominators.

The scope of the present paper is to review the main features of the novel reduction algorithm and demonstrate its performance on a selection of challenging calculations of scattering amplitudes with massive bosons and quarks, involving *six*, *seven*, and *eight* particles. The integrand-reduction via Laurent expansion has been implemented in the C++ library NINJA [82], and interfaced to the GoSAM framework [12] for the evaluation of virtual one-loop scattering amplitudes. The cleaner and lighter system-solving strategy, which deals with a diagonal system instead of a triangular one, and which substitutes the polynomial subtractions with coefficients corrections, turns into net gains in terms of both numerical accuracy and computing speed. We recall that the new library has been recently used in the evaluation of NLO QCD corrections to $pp \to t\bar{t}Hj$ [45].

The paper is organized as follows. In section 2, we discuss the theoretical foundations of the integrand decomposition via Laurent expansion, and its implementation in an algorithm for the reduction of one-loop amplitudes. The description of the interface between NINJA and GoSAM for automated one-loop calculation is discussed in section 3. Section 4 is devoted to a detailed study of the precision and of the computational performance of the novel framework, which shows a significant improvement with respect to the standard algorithms. Applications of the GoSAM+NINJA framework to the evaluation of NLO QCD virtual correction to several multi-leg massive processes are shown in section 5.

2 Reduction algorithm — integrand reduction via Laurent expansion

In this section we describe the *Laurent-expansion method* for the integrand reduction of one-loop amplitudes as implemented in the C++ library NINJA.

2.1 Integrand and integral decomposition

An n-point one-loop amplitude can be written as a linear combination of contributions $\mathcal{M}_{1\cdots n}$ of the form

$$\mathcal{M}_{1\cdots n} = \int d^d\bar{q}\, \mathcal{I}_{1\cdots n} = \int d^d\bar{q}\, \frac{\mathcal{N}(\bar{q})}{D_1 \cdots D_n} \tag{2.1}$$

where $\mathcal{N}(\bar{q})$ is a process-dependent polynomial numerator in the components of the $d = (4 - 2\epsilon)$-dimensional loop momentum $\bar{q}$. The latter can be decomposed as follows,

$$\bar{\slashed{q}} = \slashed{q} + \slashed{\mu}\,, \qquad \bar{q}^2 = q^2 - \mu^2\,, \tag{2.2}$$

in terms of its 4-dimensional component, q, and μ^2 which encodes its (-2ϵ)-dimensional components. The denominators D_i are quadratic polynomials in $\bar{q}$ and correspond to

Feynman loop propagators,

$$D_i = (\bar{q} + p_i)^2 - m_i^2. \tag{2.3}$$

Every one-loop integrand in d dimensions can be decomposed as [6, 73]

$$\mathcal{I}_{1\cdots n} \equiv \frac{\mathcal{N}_{1\cdots n}}{D_1 \ldots D_n} = \sum_{k=1}^{5} \sum_{\{i_1,\cdots,i_k\}} \frac{\Delta_{i_1\cdots i_k}}{D_{i_1} \cdots D_{i_k}}, \tag{2.4}$$

where the $\Delta_{i_1\cdots i_k}$ are irreducible polynomial residues, i.e. polynomials which do not contain any term proportional to the corresponding loop denominators $D_{i_1}, \ldots, D_{i_k}$. The second sum in eq. (2.4) runs over all unordered selections without repetition of the k indices $\{i_1, \cdots, i_k\}$.

For any set of denominators $D_{i_1}, \ldots, D_{i_k}$ with $k \leq 5$, one can choose a 4-dimensional basis of momenta $\mathcal{E} = \{e_1, e_2, e_3, e_4\}$ which satisfies the following normalization conditions

$$e_1 \cdot e_2 = 1, \qquad e_3^2 = e_4^2 = \delta_{k4}, \qquad e_3 \cdot e_4 = -(1 - \delta_{k4}), \tag{2.5}$$

while all the other scalar products vanish. In addition, for $k = 4$ we choose the basis such that e_4 is orthogonal to the external legs of the sub-diagram identified by the set of denominators in consideration. Similarly, for $k = 2, 3$ we choose both e_3 and e_4 to be orthogonal to the external legs of the corresponding sub-diagram. With this choices of momentum basis, the numerator and the denominators can be written as polynomials in the coordinates $\mathbf{z} \equiv (z_1, z_2, z_3, z_4, z_5) = (x_1, x_2, x_3, x_4, \mu^2)$. The variables x_i are the components of q with respect to the basis $\mathcal{E}$,

$$q^\nu = -p_{i_1}^\nu + x_1\ e_1^\nu + x_2\ e_2^\nu + x_3\ e_3^\nu + x_4\ e_4^\nu\ . \tag{2.6}$$

More explicitly, the numerator is a polynomial in the components of q and μ^2

$$\mathcal{N}(\bar{q}) = \mathcal{N}(q, \mu^2) = \mathcal{N}(x_1, x_2, x_3, x_4, \mu^2) = \mathcal{N}(\mathbf{z}). \tag{2.7}$$

The coordinates x_i can also be written as scalar products,

$$\begin{aligned}
x_1 &= (q + p_{i_1}) \cdot e_2 \\
x_2 &= (q + p_{i_1}) \cdot e_1 \\
x_3 &= -((q + p_{i_1}) \cdot e_4)(1 - \delta_{k4}) + ((q + p_{i_1}) \cdot e_3)\delta_{k4} \\
x_4 &= -((q + p_{i_1}) \cdot e_3)(1 - \delta_{k4}) + ((q + p_{i_1}) \cdot e_4)\delta_{k4}.
\end{aligned} \tag{2.8}$$

With these definitions, one can show [6, 51, 73] that the most general parametric form

of a residue in a renormalizable theory is

$$\Delta_{i_1 i_2 i_3 i_4 i_5} = c_0^{(i_1 i_2 i_3 i_4 i_5)} \mu^2$$

$$\Delta_{i_1 i_2 i_3 i_4} = c_0^{(i_1 i_2 i_3 i_4)} + c_1^{(i_1 i_2 i_3 i_4)} x_4 + \mu^2 \left(c_2^{(i_1 i_2 i_3 i_4)} + c_3^{(i_1 i_2 i_3 i_4)} x_4 + \mu^2 c_4^{(i_1 i_2 i_3 i_4)} \right)$$

$$\Delta_{i_1 i_2 i_3} = c_0^{(i_1 i_2 i_3)} + c_1^{(i_1 i_2 i_3)} x_3 + c_2^{(i_1 i_2 i_3)} x_3^2 + c_3^{(i_1 i_2 i_3)} x_3^3 + c_4^{(i_1 i_2 i_3)} x_4 + c_5^{(i_1 i_2 i_3)} x_4^2$$
$$+ c_6^{(i_1 i_2 i_3)} x_4^3 + \mu^2 \left(c_7^{(i_1 i_2 i_3)} + c_8^{(i_1 i_2 i_3)} x_3 + c_9^{(i_1 i_2 i_3)} x_4 \right)$$

$$\Delta_{i_1 i_2} = c_0^{(i_1 i_2)} + c_1^{(i_1 i_2)} x_2 + c_2^{(i_1 i_2)} x_3 + c_3^{(i_1 i_2)} x_4 + c_4^{(i_1 i_2)} x_2^2 + c_5^{(i_1 i_2)} x_3^2$$
$$+ c_6^{(i_1 i_2)} x_4^2 + c_7^{(i_1 i_2)} x_2 x_3 + c_8^{(i_1 i_2)} x_2 x_4 + c_9^{(i_1 i_2)} \mu^2$$

$$\Delta_{i_1} = c_0^{(i_1)} + c_1^{(i_1)} x_1 + c_2^{(i_1)} x_2 + c_3^{(i_1)} x_3 + c_4^{(i_1)} x_4. \tag{2.9}$$

This parametric form can also be extended to non-renormalizable and effective theories, where the rank of the numerator can be larger than the number of loop propagators [78]. Most of the term appearing in eq. (2.9) vanish after integration, i.e. they are *spurious*. The non-spurious coefficients, instead, appear in the final result which expresses the amplitude $\mathcal{M}_{1\cdots n}$ as a linear combination of known Master Integrals,

$$\mathcal{M}_{1\cdots n} = \sum_{\{i_1, i_2, i_3, i_4\}} \left\{ c_0^{(i_1 i_2 i_3 i_4)} I_{i_1 i_2 i_3 i_4} + c_4^{(i_1 i_2 i_3 i_4)} I_{i_1 i_2 i_3 i_4}[\mu^4] \right\}$$
$$+ \sum_{\{i_1, i_2, i_3\}}^{n-1} \left\{ c_0^{(i_1 i_2 i_3)} I_{i_1 i_2 i_3} + c_7^{(i_1 i_2 i_3)} I_{i_1 i_2 i_3}[\mu^2] \right\}$$
$$+ \sum_{\{i_1, i_2\}} \left\{ c_0^{(i_1 i_2)} I_{i_1 i_2} + c_1^{(i_1 i_2)} I_{i_1 i_2}[(q + p_{i_1}) \cdot e_2] \right.$$
$$\left. + c_2^{(i_1 i_2)} I_{i_1 i_2}[((q + p_{i_1}) \cdot e_2)^2] + c_9^{(i_1 i_2)} I_{i_1 i_2}[\mu^2] \right\}$$
$$+ \sum_{i_1} c_0^{(i_1)} I_{i_1}, \tag{2.10}$$

where

$$I_{i_1 \cdots i_k}[\alpha] \equiv \int d^d \bar{q} \frac{\alpha}{D_{i_1} \cdots D_{i_k}}, \qquad I_{i_1 \cdots i_k} \equiv I_{i_1 \cdots i_k}[1].$$

The problem of the computation of any one-loop amplitude can therefore be reduced to the problem of the determination of the coefficients of the Master Integrals appearing in eq. (2.10), which in turn can be identified with a subset of the coefficients of the parametric residues in eq. (2.9).

2.2 Scattering amplitudes via Laurent expansion

In ref. [78], elaborating on the the techniques proposed in [80, 81], an improved version of the integrand-reduction method for one-loop amplitudes was presented. This method allows, whenever the analytic dependence of the integrand on the loop momentum is known,

to extract the unknown coefficients of the residues $\Delta_{i_1\cdots i_k}$ by performing a Laurent expansion of the integrand with respect to one of the free loop components which are not constrained by the corresponding on-shell conditions $D_{i_1} = \cdots = D_{i_k} = 0$.

Within the original integrand reduction algorithm [61, 62, 64], the determination of these unknown coefficients requires: *i)* to sample the numerator on a finite subset of the on-shell solutions; *ii)* to subtract from the integrand the non-vanishing contributions coming from higher-point residues; and *iii)* to solve the resulting linear system of equations.

With the Laurent-expansion approach, since in the asymptotic limit both the integrand and the higher-point subtractions exhibit the same polynomial behavior as the residue, one can instead identify the unknown coefficients with the ones of the expansion of the integrand, corrected by the contributions coming from higher-point residues. In other words, the system of equations for the coefficients becomes diagonal and the subtractions of higher-point contributions can be implemented as *corrections at the coefficient level* which replace the subtractions at the integrand level of the original algorithm. Because of the universal structure of the residues, the parametric form of these corrections can be computed once and for all, in terms of a subset of the higher-point coefficients. This also allows to significantly reduce the number of coefficients entering in each subtraction. For instance, box and pentagons do not affect at all the computation of lower-points residues. In the followings, we describe in more detail how to determine the needed coefficients of each residue.

Pentagons. Pentagons contributions are spurious, i.e. they do not appear in the integrated result. In the original integrand reduction algorithm their computation is nevertheless needed, in order to implement the corresponding subtractions at the integrand level. Within the Laurent expansion approach, since the subtraction terms of five-point residues always vanish in the asymptotic limit, their computation is instead not needed and can be skipped.

Boxes. The coefficient c_0 of the box contributions can be determined via 4-dimensional quadruple cuts [4]. In four dimensions (i.e. $\bar{q} = q$, $\mu^2 = 0$) a quadruple cut $D_{i_1} = \cdots = D_{i_4} = 0$ has two solutions, q_+ and q_-. The coefficient c_0 can be expressed in terms of these solutions as

$$c_0^{(i_1 i_2 i_3 i_4)} = \frac{1}{2} \left(\left. \frac{\mathcal{N}(q)}{\prod_{j \neq i_1, i_2, i_3, i_4} D_j} \right|_{q=q_+} + \left. \frac{\mathcal{N}(q)}{\prod_{j \neq i_1, i_2, i_3, i_4} D_j} \right|_{q=q_-} \right). \tag{2.11}$$

The coefficient c_4 can be found by evaluating the integrand on d-dimensional quadruple cuts in the asymptotic limit $\mu^2 \to \infty$ [81]. A d-dimensional quadruple cut has an infinite number of solutions which can be parametrized by the extra-dimensional variable μ^2. These solutions become particularly simple in the limit of large μ^2, namely

$$q_\pm^\nu = a^\nu \pm \sqrt{\mu^2 + \beta} \, e_4^\nu \stackrel{\mu^2 \to \infty}{\longrightarrow} \pm \sqrt{\mu^2} \, e_4^\nu + \mathcal{O}(1) \tag{2.12}$$

where the vector a^ν and the constant β are fixed by the cut conditions. The coefficient c_4, when non-vanishing, can be found in this limit as the leading term of the expansion of the

integrand

$$\frac{\mathcal{N}(q,\mu^2)}{\prod_{j\neq i_1,i_2,i_3,i_4} D_j} \overset{\mu^2\to\infty}{\longrightarrow} c_4^{(i_1 i_2 i_3 i_4)}\,\mu^4 + \mathcal{O}(\mu^3). \tag{2.13}$$

The other coefficients of the boxes are spurious and their computation can be avoided.

Triangles. The residues of the triangle contributions can be determined by evaluating the integrand on the solutions of d-dimensional triple cuts [80], which can be parametrized by the extra-dimensional variable μ^2 and another parameter t,

$$q_+ = a^\nu + t\,e_3^\nu + \frac{\beta+\mu^2}{2\,t}\,e_4^\nu, \qquad q_- = a^\nu + \frac{\beta+\mu^2}{2\,t}\,e_3^\nu + t\,e_4^\nu, \tag{2.14}$$

where the vector a^ν and the constant β are fixed by the cut conditions $D_{i_1} = D_{i_2} = D_{i_3} = 0$. On these solutions, the integrand generally receives contributions from the residue of the triple cut $\Delta_{i_1 i_2 i_3}$, as well as from the boxes and pentagons which share the three cut denominators. However, after taking the asymptotic expansion at large t and dropping the terms which vanish in this limit, the pentagon contributions vanish, while the box contributions are constant in t but vanish when taking the average between the parametrizations q_+ and q_- of eq. (2.14). More explicitly,

$$\frac{\mathcal{N}(q_\pm,\mu^2)}{\prod_{j\neq i_1,i_2,i_3} D_j} = \Delta_{i_1 i_2 i_3} + \sum_j \frac{\Delta_{i_1 i_2 i_3 j}}{D_j} + \sum_{jk} \frac{\Delta_{i_1 i_2 i_3 jk}}{D_j D_k}$$
$$= \Delta_{i_1 i_2 i_3} + d_1^\pm + d_2^\pm\,\mu^2 + \mathcal{O}(1/t), \qquad \text{with } d_i^+ + d_i^- = 0. \tag{2.15}$$

Moreover, even though the integrand is a rational function, in this asymptotic limit it exhibits the same polynomial behavior as the expansion of the residue $\Delta_{i_1 i_2 i_3}$,

$$\frac{\mathcal{N}(q_+,\mu^2)}{\prod_{j\neq i_1,i_2,i_3} D_j} = n_0^+ + n_7^+\,\mu^2 - (n_4 + n_9\,\mu^2)\,t + n_5\,t^2 + n_6\,t^3 + \mathcal{O}(1/t)$$

$$\frac{\mathcal{N}(q_-,\mu^2)}{\prod_{j\neq i_1,i_2,i_3} D_j} = n_0^- + n_7^-\,\mu^2 - (n_1 + n_8\,\mu^2)\,t + n_2\,t^2 + n_3\,t^3 + \mathcal{O}(1/t) \tag{2.16}$$

$$\Delta_{i_1 i_2 i_3}(q_+,\mu^2) = c_0^{(i_1 i_2 i_3)} + c_7^{(i_1 i_2 i_3)}\,\mu^2 - (c_4^{(i_1 i_2 i_3)} + c_9^{(i_1 i_2 i_3)}\,\mu^2)\,t$$
$$+ c_5^{(i_1 i_2 i_3)}\,t^2 - c_6^{(i_1 i_2 i_3)}\,t^3 + \mathcal{O}(1/t)$$

$$\Delta_{i_1 i_2 i_3}(q_-,\mu^2) = c_0^{(i_1 i_2 i_3)} + c_7^{(i_1 i_2 i_3)}\,\mu^2 - (c_1^{(i_1 i_2 i_3)} + c_8^{(i_1 i_2 i_3)}\,\mu^2)\,t$$
$$+ c_2^{(i_1 i_2 i_3)}\,t^2 - c_3^{(i_1 i_2 i_3)}\,t^3 + \mathcal{O}(1/t). \tag{2.17}$$

By comparison of eqs. (2.15), (2.16) and (2.17) one gets all the triangle coefficients as

$$c_i^{(i_1 i_2 i_3)} = \frac{1}{2}(n_i^+ + n_i^-) \quad \text{for } i = 0,7, \qquad c_i^{(i_1 i_2 i_3)} = n_i \quad \text{for } i \neq 0,7. \tag{2.18}$$

It is worth to observe that, within the Laurent expansion approach, the determination of the 3-point residues does not require any subtraction of higher-point terms.

Bubbles. The on-shell solutions of a d-dimensional double cut $D_{i_1} = D_{i_2} = 0$ can be parametrized as

$$q_+ = a_0^\nu + x \, a_1^\nu + t \, e_3^\nu + \frac{\beta_0 + \beta_1 \, x + \beta_2 \, x^2 + \mu^2}{2 \, t} \, e_4^\nu,$$

$$q_- = a_0^\nu + x \, a_1^\nu + \frac{\beta_0 + \beta_1 \, x + \beta_2 \, x^2 + \mu^2}{2 \, t} \, e_3^\nu + t \, e_4^\nu, \tag{2.19}$$

in terms of the three free parameters x, t and μ^2, while the vectors a_i^ν and the constants β_i are fixed by the on-shell conditions. After evaluating the integrand on these solutions and taking the asymptotic limit $t \to \infty$, the only non-vanishing subtraction terms come from the triangle contributions,

$$\frac{\mathcal{N}(q_\pm, \mu^2)}{\prod_{j \neq i_1, i_2} D_j} = \Delta_{i_1 i_2} + \sum_j \frac{\Delta_{i_1 i_2 j}}{D_j} + \sum_{jk} \frac{\Delta_{i_1 i_2 jk}}{D_j D_k} + \sum_{jkl} \frac{\Delta_{i_1 i_2 jkl}}{D_j D_k D_l}$$

$$= \Delta_{i_1 i_2} + \sum_j \frac{\Delta_{i_1 i_2 j}}{D_j} + \mathcal{O}(1/t). \tag{2.20}$$

The integrand and the subtraction term are rational function, but in the asymptotic limit they both have the same polynomial behavior as the residue, namely

$$\frac{\mathcal{N}(q_+, \mu^2)}{\prod_{j \neq i_1, i_2} D_j} = n_0 + n_9 \, \mu^2 + n_1 \, x + n_2 \, x^2 - (n_5 + n_8 x) t + n_6 \, t^2 + \mathcal{O}(1/t)$$

$$\frac{\mathcal{N}(q_-, \mu^2)}{\prod_{j \neq i_1, i_2} D_j} = n_0 + n_9 \, \mu^2 + n_1 \, x + n_2 \, x^2 - (n_3 + n_7 x) t + n_4 \, t^2 + \mathcal{O}(1/t) \tag{2.21}$$

$$\frac{\Delta_{i_1 i_2 j}(q_+, \mu^2)}{D_j} = c_{s,0}^{(j)} + c_{s,9}^{(j)} \mu^2 + c_{s,1}^{(j)} x + c_{s,2}^{(j)} x^2 - (c_{s,5}^{(j)} + c_{s,8}^{(j)} x) t + c_{s,6}^{(j)} t^2 + \mathcal{O}(1/t)$$

$$\frac{\Delta_{i_1 i_2 j}(q_-, \mu^2)}{D_j} = c_{s,0}^{(j)} + c_{s,9}^{(j)} \mu^2 + c_{s,1}^{(j)} x + c_{s,2}^{(j)} x^2 - (c_{s,3}^{(j)} + c_{s,7}^{(j)} x) t + c_{s,4}^{(j)} t^2 + \mathcal{O}(1/t) \tag{2.22}$$

$$\Delta_{i_1 i_2}(q_+, \mu^2) = c_0^{(i_1 i_2)} + c_9^{(i_1 i_2)} \mu^2 + c_1^{(i_1 i_2)} x + c_2^{(i_1 i_2)} x^2 - (c_5^{(i_1 i_2)} + c_8^{(i_1 i_2)} x) \, t$$

$$+ c_6^{(i_1 i_2)} \, t^2 + \mathcal{O}(1/t)$$

$$\Delta_{i_1 i_2}(q_-, \mu^2) = c_0^{(i_1 i_2)} + c_9^{(i_1 i_2)} \mu^2 + c_1^{(i_1 i_2)} x + c_2^{(i_1 i_2)} x^2 - (c_3^{(i_1 i_2)} + c_7^{(i_1 i_2)} x) \, t$$

$$+ c_4^{(i_1 i_2)} \, t^2 + \mathcal{O}(1/t). \tag{2.23}$$

The coefficients $c_{s,i}^{(j)}$ of the Laurent expansion of the subtractions terms in eqs. (2.22) can be computed once and for all as parametric functions of the triangles coefficients. Therefore, the subtraction of the triangles can be implemented as corrections to the coefficients of the expansion of the integrand. Indeed, by inserting eqs. (2.21), (2.22) and (2.23) in eq. (2.20) one gets

$$c_i^{(i_1 i_2)} = n_i - \sum_j c_{s,i}^{(j)} \quad \text{for } i = 0, \dots, 9. \tag{2.24}$$

Tadpoles. Once the coefficients of the triangles and the bubbles are known, one can determine the non-spurious coefficient c_0 of a tadpole residue Δ_{i_1} by evaluating the integrand on the single cut $D_{i_1} = 0$. One can choose 4-dimensional solutions of the form

$$q_+^\nu = -p_{i_1}^\nu + t\, e_3^\nu + \frac{\beta}{2\,t}\, e_4^\nu \qquad (2.25)$$

parametrized by the free variable t, while the constant β is fixed by the cut conditions. In the asymptotic limit $t \to \infty$, only bubbles and triangles coefficients are non-vanishing,

$$
\begin{aligned}
\frac{\mathcal{N}(q_+)}{\prod_{j \neq i_1} D_j} &= \Delta_{i_1} + \sum_j \frac{\Delta_{i_1 j}}{D_j} + \sum_{jk} \frac{\Delta_{i_1 jk}}{D_j D_k} + \sum_{jkl} \frac{\Delta_{i_1 jkl}}{D_j D_k D_l} \\
&= \Delta_{i_1} + \sum_j \frac{\Delta_{i_1 j}}{D_j} + \sum_{jk} \frac{\Delta_{i_1 jk}}{D_j D_k} + \mathcal{O}(1/t).
\end{aligned} \qquad (2.26)
$$

Similarly to the case of the bubbles, in this limit the integrand and the subtraction terms exhibit the same polynomial behavior as the residue, i.e.

$$\frac{\mathcal{N}(q_+)}{\prod_{j \neq i_1} D_j} = n_0 - n_4\, t + \mathcal{O}(1/t) \qquad (2.27)$$

$$\frac{\Delta_{i_1 j}(q_+)}{D_j} = c_{s_2,0}^{(j)} - c_{s_2,4}^{(j)}\, t + \mathcal{O}(1/t) \qquad (2.28)$$

$$\frac{\Delta_{i_1 jk}(q_+)}{D_j D_k} = c_{s_3,0}^{(jk)} - c_{s_3,4}^{(jk)}\, t + \mathcal{O}(1/t) \qquad (2.29)$$

$$\Delta_{i_1}(q_+) = c_0^{(i_1)} - c_4^{(i_1)}\, t. \qquad (2.30)$$

Putting everything together, we can write the coefficient of the tadpole integral as the corresponding one in the expansion of the integrand, corrected by coefficient-level subtractions

$$c_0^{(i_1)} = n_0 - \sum_j c_{s_2,0}^{(j)} - \sum_{jk} c_{s_3,0}^{(jk)}. \qquad (2.31)$$

Once again, we observe that the subtraction terms $c_{s_2,0}^{(j)}$ and $c_{s_3,0}^{(jk)}$, coming from bubbles and triangles contributions respectively, are known parametric functions of the coefficients of the corresponding higher-point residues.

2.3 The C++ library NINJA

The C++ library NINJA [82] provides a semi-numerical implementation of the Laurent expansion method described above. Since the integrand is a rational function of the loop variables, its Laurent expansion is performed via a simplified polynomial division algorithm between the expansion of the numerator $\mathcal{N}$ and the uncut denominators.

The inputs of the reduction algorithm implemented in NINJA are the external momenta p_i and the masses m_i of the loop denominators defined in eq. (2.3), and the numerator $\mathcal{N}(q, \mu^2)$ of the integrand cast in four different forms.

- The first form provides a simple evaluation of the numerator as a function of q and μ^2, which is used in order to compute the coefficient c_0 of the boxes. It can also be used in order to compute the spurious coefficients of the pentagons via penta-cuts, and all the ones of the boxes when the expansion in μ^2 is not provided.

The other three forms of the numerator yield instead the leading terms of a parametric expansion of the integrand.

- The first expansion is the one used in order to obtain the coefficient c_4 of the boxes. When the rank r is equal to the number n of external legs of the diagram, this method returns the coefficient of t^n obtained by substituting in the numerator $\mathcal{N}(q, \mu^2)$

$$q^\nu \to t\, v^\nu, \qquad \mu^2 \to t^2\, v^2 \tag{2.32}$$

as a function of a generic vector v, which is computed by NINJA and is determined by the quadruple-cut constraints.

- The second expansion is used in order to compute triangles and tadpole coefficients. In this case it returns coefficients of the terms $t^j \mu^{2k}$ for $j = r, r-1, \ldots, n-3$, obtained from $\mathcal{N}(q, \mu^2)$ with the substitutions

$$q^\nu \to v_0^\nu + t\, v_3^\nu + \frac{\beta + \mu^2}{t}\, v_4^\nu, \qquad v_3^2 = v_4^2 = 0, \tag{2.33}$$

as a function of the generic momenta v_i^ν and the constant β_0. Since in a renormalizable theory $r \le n$, and by definition of rank we have $j + 2k \le r$, at most 6 terms can be non-vanishing in the specified range of j. For effective theories with $r \le n+1$, one can have instead up to 9 non-vanishing polynomial terms. In each call of the numerator, NINJA specifies the lowest power of t which is needed in the evaluation, avoiding thus the computation of unnecessary coefficients of the expansion.

- The third and last expansion is needed for the computation of the 2-point residues and returns the coefficients of the terms $t^j \mu^{2k} x^l$ for $j = r, r-1, \ldots, n-2$, obtained from $\mathcal{N}(q, \mu^2)$ with the substitutions

$$q^\nu \to v_1^\nu + x\, v_2^\nu + t\, v_3^\nu + \frac{\beta_0 + \beta_1\, x + \beta_2\, x^2 + \mu^2}{t}\, v_4^\nu, \quad v_2 \cdot v_3 = v_2 \cdot v_4 = v_3^2 = v_4^2 = 0, \tag{2.34}$$

as a function of the cut-dependent momenta v_i^ν and constants β_i. In a renormalizable theory one can have at most 7 non-vanishing terms in this range of j, while for $r \le n+1$ one can have 13 non-vanishing terms. As in the previous case, in each call of the numerator, NINJA specifies the lowest power of t which is needed. It is worth to notice that the expansion in eq. (2.34) can be obtained from the previous one in eq. (2.33) with the substitutions

$$v_0^\nu \to v_1^\nu + x\, v_2^\nu, \qquad \beta \to \beta_0 + \beta_1\, x + \beta_2\, x^2, \qquad v_2 \cdot v_3 = v_2 \cdot v_4 = 0.$$

All these expansions can be easily and quickly obtained from the knowledge of the analytic dependence of the loop momentum on q and μ^2. For every phase-space point, NINJA computes the parametric solutions of all the multiple cuts, performs the Laurent expansion of the integrand via a simplified polynomial division between the expansion of the numerator and the set of the uncut denominators, and implements the subtractions at the coefficient level appearing in eqs. (2.24) and (2.31). Finally, the obtained non-spurious coefficients are multiplied by the corresponding Master Integrals in order to get the integrated result as in eq. (2.10).

The routines which compute the Master Integrals are called by NINJA via a generic interface which allows to use any integral library implementing it, with the possibility of switching between different libraries at run-time. By default, a C++ wrapper of the ONELOOP integral library [83, 84] is used. This wrapper caches every computed integral allowing constant time lookups of their values from their arguments. An interface with the LOOPTOOLS [85, 86] library is available as well.

The NINJA library can also be used in order to compute integrals from effective and non-renomalizable theories where the rank r of the numerator can exceed the number of legs by one unit. An example of this application, given in section 5, is Higgs boson production plus three jets in gluon fusion, in the effective theory defined by the infinite top-mass limit.

3 Interfacing NINJA with GoSam

The library NINJA has been interfaced with the automatic generator of one-loop amplitudes GoSam. The latter provides NINJA with analytic expressions for the integrands of one-loop Feynman diagrams for generic processes within the Standard Model and also for Beyond Standard Model theories.

GoSam combines automated diagram generation and algebraic manipulation [87–90] with integrand-reduction techniques [6, 63–65, 73, 78]. Amplitudes are generated via Feynman diagrams, using QGRAF [87], FORM [88], SPINNEY [90] and HAGGIES [89].

After the generation of all contributing diagrams, the virtual corrections are evaluated using the d-dimensional integrand-level reduction method, as implemented in the library SAMURAI [62], which allows for the combined determination of both cut-constructible and rational terms at once. As an alternative, the tensorial decomposition provided by GOLEM95C [91–93] is also available. Such reduction, which is numerically stable but more time consuming, is employed as a rescue system. After the reduction, all relevant master integrals can be computed by means of GOLEM95C [93], QCDLOOP [94, 95], or ONELOOP [83].

The possibility to deal with higher-rank one-loop integrals, where powers of loop momenta in the numerator exceed the number of denominators, is implemented in all three reduction programs SAMURAI [78, 79], NINJA and GOLEM95C [96]. Higher rank integrals can appear when computing one-loop integrals in effective-field theories, e.g. for calculations involving the effective gluon-gluon-Higgs vertex [42, 44], or when dealing with spin-2 particles [41].

In order to embed Ninja into the GoSam framework, the algebraic manipulation of the integrands was adapted to generate the expansions needed by Ninja and described in section 2.3. The numerator, in all its forms, is then optimized for fast numerical evaluation by exploiting the new features of Form 4 [97, 98], and written in a Fortran90 source file which is compiled. At running time, these expressions are used as input for Ninja.

The Fortran90 module of the interface between Ninja and GoSam defines subroutines which allow to control some of the settings of Ninja directly from settings of the code that generated the virtual part of the amplitudes. Upon importing the module, the user can change the integral library used by Ninja choosing between the use of OneLoop [83] and the LoopTools [85, 86].

For debugging purposes, one can also ask Ninja to perform some internal test or print some information about the ongoing computation. This option allows to choose among different internal tests, namely the global $\mathcal{N} = \mathcal{N}$ test, the local $\mathcal{N} = \mathcal{N}$ tests on different cuts, or a combination of both. These tests have been described in [62]. The verbosity of the debug output can be adjusted to control the amount of details printed out in the output file, for example the final results for the finite part and the poles of the diagram, the values of the coefficients that are computed in the reduction, the values of the corresponding Master Integrals, and the results of the various internal tests.

4 Precision tests

Within the context of numerical and semi-numerical techniques, the problem of estimating correctly the precision of the results is of primary importance. In particular, when performing the phase space integration of the virtual contribution, it is important to assess in real time, for each phase space point, the level of precision of the corresponding one-loop matrix element.

Whenever a phase space point is found in which the quality of the result falls below a certain threshold, either the point is discarded or the evaluation of the amplitude is repeated by means of a safer, albeit less efficient procedure. Examples of such a method involve the use of higher precision routines, or in the case of GoSam the use of traditional tensorial reconstruction of the amplitude, provided by Golem95C.

Various techniques for detecting points with low precision have been implemented within the different automated tools for the evaluation of one-loop virtual corrections.

A standard method which is widely employed is based on the comparison between the numerical values of the poles with their known analytic results dictated by the universal behavior of the infrared singularities. While this method is quite reliable, not all integrals which appear in the reconstruction of the amplitude give a contribution to the double and single poles. This often results in an overestimate of the precision, which might lead to keep phase space points whose finite part is less precise than what is predicted by the poles.

A different technique, which we refer to as *scaling test* [9], is based on the properties of scaling of scattering amplitudes when all physical scales (momenta, renormalization scale, masses) are rescaled by a common multiplicative factor x. As shown in [9], this method

provides a very good correlation between the estimated precision, and the actual precision of the finite parts.

Additional methods have been proposed, within the context of integrand-reduction approaches, which target the relations between the coefficients before integration, namely the reconstructed algebraic expressions for the numerator function before integration. This method, labeled $\mathcal{N} = \mathcal{N}$ test [61, 62], can be applied to the full amplitude (global $\mathcal{N} = \mathcal{N}$ test) or individually within each residue of individual cuts (local $\mathcal{N} = \mathcal{N}$ test). The drawback of this technique comes from the fact that the test is applied at the level of individual diagrams, rather than on the final result summed over all diagrams, making the construction of a rescue system quite cumbersome.

For the precision analysis contained in this paper, we present a new simple and efficient method for the estimation of the number of digits of precision in the results, which we call *rotation test*. This new method exploits the invariance of the scattering amplitudes under an azimuthal rotation about the beam axis, namely the direction of the initial colliding particles.

Such a rotation, which does not affect the initial states, changes the momenta of all final particles without changing their relative position, thus reconstructing a theoretically identical process. However, the change in the values of all final state external momenta is responsible for different bases for the parametrization of the residues within the integrand reconstruction, different coefficients in front of the master integrals, as well as different numerical values when the master integrals are computed. We tested that the choice of the angle of rotation does not affect the estimate, as long as this angle is not too small.

In order to study the correlation of the error estimated by the rotation test and the exact error, we follow the strategy of ref. [9]. In particular, we generated 10^4 points for the process $u\bar{d} \to Wb\bar{b}g$ with massive bottom quarks, both in quadrupole and standard double precision, which we label with A_{quad} and A respectively, as well as the same points in double precision after performing a rotation, called A_{rot}.

We define the exact error δ_{ex} as

$$\delta_{\mathrm{ex}} = \left| \frac{A_{\mathrm{quad}} - A}{A_{\mathrm{quad}}} \right| , \tag{4.1}$$

and the estimated error δ_{rot} as

$$\delta_{\mathrm{rot}} = 2 \left| \frac{A_{\mathrm{rot}} - A}{A_{\mathrm{rot}} + A} \right| . \tag{4.2}$$

In figure 1, we plot the distribution of the quantity

$$\mathcal{C} = \frac{\log_{10}(\delta_{\mathrm{rot}})}{\log_{10}(\delta_{\mathrm{ex}})} - 1 , \tag{4.3}$$

evaluated for each phase space point. In the ideal case of a perfect correlation between the exact error, as estimated by the quadrupole precision result, and the error estimated by the less time-consuming rotation test, the value of $\mathcal{C}$ would be close to zero, while the spread of the distribution can provide a picture of the degree of correlation. Moreover, we observe a similar behavior for the rotation and the scaling tests.
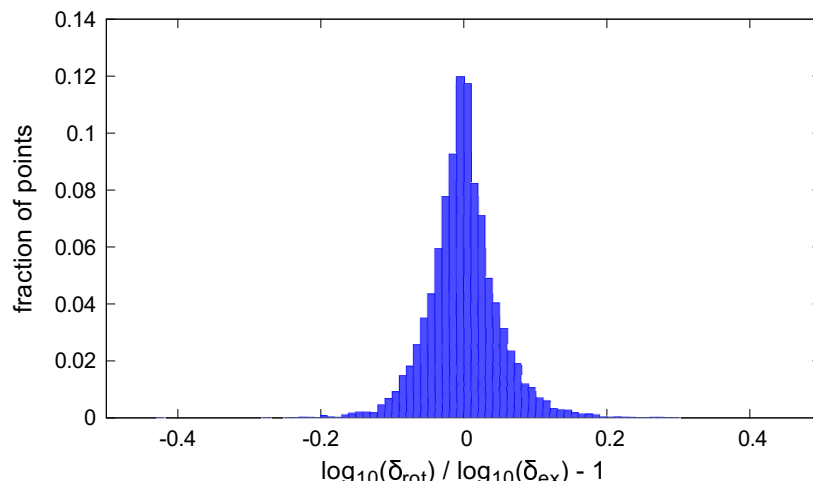
Figure 1. Correlation plot based on 10^4 points for the process $u\bar{d} \to Wb\bar{b}g$ with massive bottom quarks.

In the following, we will employ the rotation test as the standard method to estimate the precision of the finite part of each renormalized virtual matrix elements. If we call δ_0 the error at any given phase space point and calculate it according to eq. (4.2), we can define the precision of the finite part as $P_0 = \log_{10}(\delta_0)$. Concerning the precision of the double and single poles, $P_{-2} = \log_{10}(\delta_{-2})$ and $P_{-1} = \log_{10}(\delta_{-1})$, we employ the fact that the values of the pole coefficients, after renormalization, are solely due to infrared (IR) divergencies, whose expressions are well known [99]. δ_{-2} and δ_{-1} are defined using formula in eq. (4.1), in which the exact values are provided by the reconstructed IR poles, which is automatically evaluated by GoSam.

In order to assess the level of precision of the results obtained with Ninja within GoSam, in figures 2 and 3, we plot the distributions of P_{-2} (precision of the double pole), P_{-1} (single pole) and P_0 (finite part) for two challenging virtual amplitudes with massive internal and external particles, namely $gg \to t\bar{t}Hg$ ($t\bar{t}Hj$) and $u\bar{u} \to Hu\bar{u}gg$ ($Hjjjj$) in VBF. By selecting an upper bound on the value of P_0, we can set a *rejection criterium* for phase space points in which the quality of the calculated scattering amplitudes falls below the requested precision. This also allows to estimate the percentage of points which would be discarded (or redirected to the rescue system). This value, as expected by analyzing the shape of the various distributions, is strongly process dependent and should be selected according to the particular phenomenological analysis at hand. As a benchmark value, in ref. [9], the threshold for rejection was set to $P_0 = -3$. In a similar fashion, in table 1, we provide the percentages of *bad points*, which are points whose precision falls below the threshold, for increasing values of the rejection threshold.

The two plots are built using a set of $5 \cdot 10^4$ and $1 \cdot 10^5$ phase space points, respectively for $gg \to t\bar{t}Hg$ and $u\bar{u} \to Hu\bar{u}gg$ (VBF). No cuts have been introduced in the selection of the points, which are randomly distributed over the whole available phase space for the outgoing particles, and are generated using RAMBO.
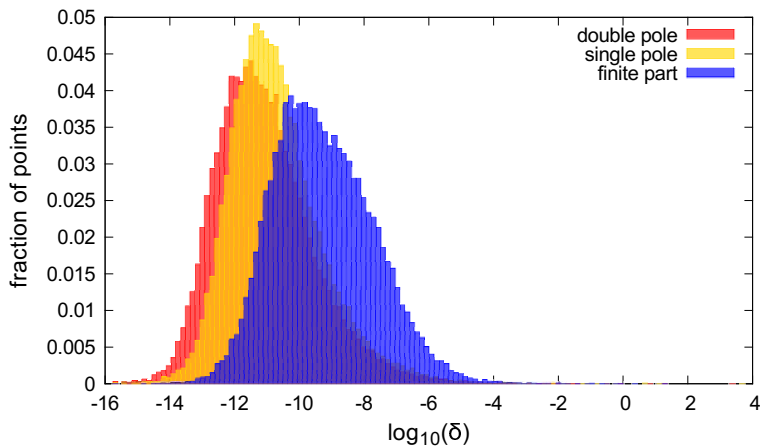
Figure 2. Precision Plot for $gg \to t\bar{t}Hg$: the distributions are obtained using $5 \cdot 10^4$ randomly distributed phase space points.
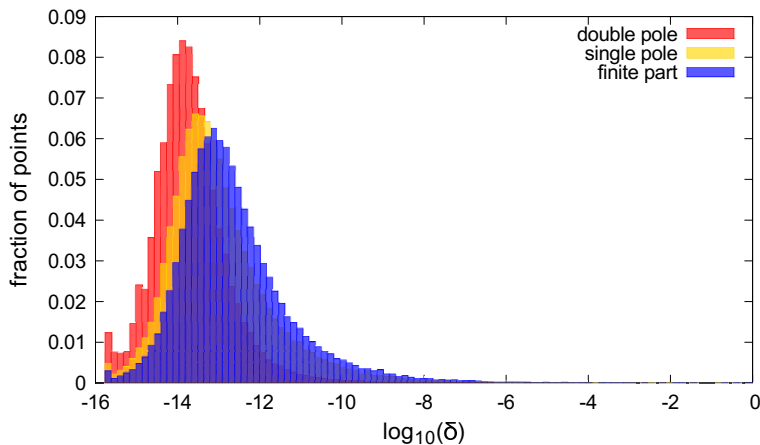

Figure 3. Precision plot for $u\bar{u} \to Hu\bar{u}gg$ in VBF: the distributions are obtained using 10^5 randomly distributed phase space points.

P_0	$u\bar{u} \to Hu\bar{u}gg$	$gg \to t\bar{t}Hg$
-3	0.02%	0.06%
-4	0.04%	0.16%
-5	0.08%	0.56%

Table 1. Percentage of bad points as a function of the rejection threshold P_0.

The use of the novel algorithm implemented in NINJA yields significant improvements both in the accuracy of results and in reduction of the computational time, due to a more efficient reduction and less frequent calls to the rescue system.

These features make GOSAM+NINJA an extremely competitive framework for massive, as well as massless, calculations. The new library has been recently used in the evaluation of NLO QCD corrections to $pp \to t\bar{t}Hj$ [45].

5 Applications to massive amplitudes

In order to demonstrate the performances of the new reduction algorithm, we apply GoSam+Ninja to a collection of processes involving *six*, *seven* and *eight* external particles. We choose processes where massive particles appear in the products of the reactions or run in the loop. We list them in table 2, and give the details of their calculations in the following subsections: for each process we provide results for a phase space point and a detailed list of the input parameters employed. While some of the considered processes have

Benchmarks: GoSam + Ninja		# NLO diagrams	ms/event
Process			
$W + 3\,j$	$d\bar{u} \to \bar{\nu}_e e^- ggg$	1 411	226
$Z + 3\,j$	$d\bar{d} \to e^+ e^- ggg$	2 928	1 911
$ZZZ + 1\,j$	$u\bar{u} \to ZZZg$	915	*12 000
$WWZ + 1\,j$	$u\bar{u} \to W^+ W^- Zg$	779	*7 050
$WZZ + 1\,j$	$u\bar{d} \to W^+ ZZg$	756	*3 300
$WWW + 1\,j$	$u\bar{d} \to W^+ W^- W^+ g$	569	*1 800
$ZZZZ$	$u\bar{u} \to ZZZZ$	408	*1 070
$WWWW$	$u\bar{u} \to W^+ W^- W^+ W^-$	496	*1 350
$t\bar{t}b\bar{b}\,(m_b \neq 0)$	$d\bar{d} \to t\bar{t}b\bar{b}$	275	178
	$gg \to t\bar{t}b\bar{b}$	1 530	5 685
$t\bar{t} + 2\,j$	$gg \to t\bar{t}gg$	4 700	13 827
$Z\,b\bar{b} + 1\,j\,(m_b \neq 0)$	$dug \to ue^+ e^- b\bar{b}$	708	*1 070
$W\,b\bar{b} + 1\,j\,(m_b \neq 0)$	$u\bar{d} \to e^+ \nu_e b\bar{b}g$	312	67
$W\,b\bar{b} + 2\,j\,(m_b \neq 0)$	$u\bar{d} \to e^+ \nu_e b\bar{b}s\bar{s}$	648	181
	$u\bar{d} \to e^+ \nu_e b\bar{b}d\bar{d}$	1 220	895
	$u\bar{d} \to e^+ \nu_e b\bar{b}gg$	3 923	5387
$WW\,b\bar{b}\,(m_b \neq 0)$	$d\bar{d} \to \nu_e e^+ \bar{\nu}_\mu \mu^- b\bar{b}$	292	115
	$gg \to \nu_e e^+ \bar{\nu}_\mu \mu^- b\bar{b}$	1 068	*5 300
$WW\,b\bar{b} + 1\,j\,(m_b = 0)$	$u\bar{u} \to \nu_e e^+ \bar{\nu}_\mu \mu^- b\bar{b}g$	3 612	*2 000
$H + 3\,j$ in GF	$gg \to Hggg$	9 325	8 961
$t\bar{t}Z + 1\,j$	$u\bar{u} \to t\bar{t}e^+ e^- g$	1408	1 220
	$gg \to t\bar{t}e^+ e^- g$	4230	19 560
$t\bar{t}H + 1\,j$	$gg \to t\bar{t}Hg$	1 517	1 505
$H + 3\,j$ in VBF	$u\bar{u} \to Hgu\bar{u}$	432	101
$H + 4\,j$ in VBF	$u\bar{u} \to Hggu\bar{u}$	1 176	669
$H + 5\,j$ in VBF	$u\bar{u} \to Hgggu\bar{u}$	15 036	29 200

Table 2. A summary of results obtained with GoSam+Ninja. Timings refer to full color- and helicity-summed amplitudes, using an Intel Core i7 CPU @ 3.40GHz, compiled with `ifort`. The timings indicated with an (*) are obtained with an Intel(R) Xeon(R) CPU E5-2650 0 @ 2.00GHz, compiled with `gfortran`.

already been studied in the literature, the virtual NLO QCD contributions to $pp \to W b\bar{b} + n$ jets $(n = 1, 2)$, $pp \to Z b\bar{b} j$, $pp \to Z t\bar{t} j$, $pp \to VVVj$ (with $V = W, Z$), $pp \to ZZZZ$, and $pp \to H + n$ jets $(n = 4, 5)$ in VBF are presented in this paper for the first time. When occurring in the final state, the *bottom* quark is treated as massive.

For calculation which were already performed with previous versions of the GoSam framework, we observe that the new reduction technique yields a significant net gain both in computing time and in accuracy. A paradigmatic example is represented by $gg \to Hggg$, whose evaluation per ps-point required approximately 20 seconds, as reported in [44], while now can be computed in less than 10 seconds.

In the following, for each of the considered scattering amplitudes, we provide a benchmark phase space point for the most involved subprocesses and, when possible, a comparison with results available in the literature. The coefficients a_i are which appear in the various tables are defined as follows:

$$\frac{a_{-2}}{\epsilon^2} + \frac{a_{-1}}{\epsilon} + a_0 \equiv \frac{2\Re\left\{\mathcal{M}^{\text{tree-level*}} \mathcal{M}^{\text{one-loop}}\right\}}{(\alpha_s/2\pi) \left|\mathcal{M}^{\text{tree-level}}\right|^2},$$

where the finite part a_0 is computed in the dimensional reduction scheme if not stated otherwise. The reconstruction of the renormalized pole can be checked against the value of a_{-1} and a_{-2} obtained by the universal singular behavior of the dimensionally regularized one-loop amplitudes [99], while the precision of the finite parts is estimated by re-evaluating the amplitudes for a set of momenta rotated by an arbitrary angle about the axis of collision, as described in section 4. The accuracy of the results obtained with GoSam+Ninja is indicated by the underlined digits.

5.1 $pp \to W + 3$ jets

Partonic process: $d\bar{u} \to \bar{\nu}_e e^- ggg$. The finite part for this process is given in the conventional dimensional regularization (CDR) scheme and was compared to the new version of NJet [16]. We also find agreement in the phase space point given by the BlackHat Collaboration [22].

PARTICLE	E	p_x	p_y	p_z
p_1	500.0000000000000000	0.0000000000000000	0.0000000000000000	500.0000000000000000
p_2	500.0000000000000000	0.0000000000000000	0.0000000000000000	-500.0000000000000000
p_3	414.1300683745429865	232.1455649459389861	332.7544367808189918	-82.9857518524426041
p_4	91.8751521026383955	-43.3570226791010995	-24.0058236140056991	77.3623460793434958
p_5	86.3540681437814044	-15.2133893202618005	37.6335512949163018	-76.2187226821854011
p_6	280.1181818093759830	-83.1261116505822031	-263.2038567586509998	47.7490851160265990
p_7	127.5225295696610033	-90.4490412959934957	-83.1783077030789002	34.0930433392580028

PARAMETER	VALUE
m_W	80.419 GeV
w_W	2.0476 GeV
N_f	5
μ	1000.0 GeV

	$d\bar{u} \to \bar{\nu}_e e^- ggg$	Ref. [16]
a_0	<u>-91.1772093904611</u>438	-91.17720939055536
a_{-1}	<u>-57.6891244440692</u>361	-57.68912444409629
a_{-2}	<u>-11.6666666666668</u>277	-11.66666666666660

Table 3. Benchmark point for the subprocess $d(p_1)\bar{u}(p_2) \to \bar{\nu}_e(p_3) e^-(p_4) g(p_5) g(p_6) g(p_7)$.

5.2 $pp \to Z + 3$ jets

Partonic process: $d\bar{d} \to e^+ e^- ggg$. The finite part for this process is given in CDR and was compared to the new version of NJET [16]. We also find agreement in the phase space point given by the BLACKHAT Collaboration [25].

PARTICLE	E	p_x	p_y	p_z
p_1	500.0000000000000000	0.0000000000000000	0.0000000000000000	500.0000000000000000
p_2	500.0000000000000000	0.0000000000000000	0.0000000000000000	-500.0000000000000000
p_3	414.1300683745429865	232.1455649459389861	332.7544367808189918	-82.9857518524426041
p_4	91.8751521026383955	-43.3570226791010995	-24.0058236140056991	77.3623460793434958
p_5	86.3540681437814044	-15.2133893202618005	37.6335512949163018	-76.2187226821854011
p_6	280.1181818093759830	-83.1261116505822031	-263.2038567586509998	47.7490851160265990
p_7	127.5225295696610033	-90.4490412959934957	-83.1783077030789002	34.0930433392580028

PARAMETER	VALUE
m_W	80.419 GeV
m_Z	91.188 GeV
w_Z	2.4414 GeV
N_f	5
μ	1000.0 GeV

	$d\bar{d} \to e^+ e^- ggg$	Ref. [16]
a_0	-91.0463291277814761	-91.04632919538757
a_{-1}	-57.6876717480941892	-57.68767174883881
a_{-2}	-11.6666666666669485	-11.66666666666667

Table 4. Benchmark point for the subprocess $d(p_1)\bar{d}(p_2) \to e^+(p_3)e^-(p_4)g(p_5)g(p_6)g(p_7)$.

5.3 $pp \to ZZZ + 1$ jet

Partonic process: $u\bar{u} \to ZZZg$.

PARTICLE	E	p_x	p_y	p_z
p_1	250.0000000000000000	0.0000000000000000	0.0000000000000000	250.0000000000000000
p_2	250.0000000000000000	0.0000000000000000	0.0000000000000000	-250.0000000000000000
p_3	98.2984277476074197	25.7992145382080409	-12.3240263933454042	23.0200218627010820
p_4	178.4558180449861595	-120.4664227955374400	-73.7638561773535599	-59.8166791207833768
p_5	142.0905125919531145	50.7287365223860434	91.2424257480069656	-31.2402050144644221
p_6	81.1552416154533205	43.9384717349430645	-5.1545431773078745	68.0368622725466565

PARAMETER	VALUE
m_W	80.376 GeV
m_Z	91.1876 GeV
N_f	5
μ	500.0 GeV

	$u\bar{u} \to ZZZg$
a_0	-18.2274687669522883
a_{-1}	-22.3832348831861125
a_{-2}	-5.6666666666670755

Table 5. Benchmark point for the subprocess $u(p_1)\bar{u}(p_2) \to Z(p_3)Z(p_4)Z(p_5)g(p_6)$.

5.4 $pp \to WWZ + 1$ jet

Partonic process: $u\bar{u} \to W^+W^-Zg$.

PARTICLE	E	p_x	p_y	p_z
p_1	250.0000000000000000	0.0000000000000000	0.0000000000000000	250.0000000000000000
p_2	250.0000000000000000	0.0000000000000000	0.0000000000000000	-250.0000000000000000
p_3	89.1058761118447791	27.0348198946258513	-12.9142626969235721	24.1225229592474193
p_4	179.7207629659015140	-126.2359378733789299	-77.2966387614043384	-62.6814876216509802
p_5	146.1313400758695593	53.1582949292336409	95.6123118862003167	-32.7363964816230890
p_6	85.0420208463841476	46.0428230495191357	-5.4014104278722739	71.2953611440265860

PARAMETER	VALUE
m_W	80.376 GeV
m_Z	91.1876 GeV
N_f	5
μ	500.0 GeV

$u\bar{u} \to W^+W^-Zg$	
a_0	-18.0050305906438837
a_{-1}	-22.1025452011781987
a_{-2}	-5.6666666666666661

Table 6. Benchmark point for the subprocess $u(p_1)\bar{u}(p_2) \to W^+(p_3)W^-(p_4)Z(p_5)g(p_6)$.

5.5 $pp \to WZZ + 1$ jet

Partonic process: $u\bar{d} \to W^+ZZg$.

PARTICLE	E	p_x	p_y	p_z
p_1	250.0000000000000000	0.0000000000000000	0.0000000000000000	250.0000000000000000
p_2	250.0000000000000000	0.0000000000000000	0.0000000000000000	-250.0000000000000000
p_3	88.8514948513947331	26.6180234830689777	-12.7151632255396141	23.7506254934495686
p_4	182.6577199093957518	-124.2897556491134168	-76.1049547854528043	-61.7151257515301381
p_5	144.7598590943426586	52.3387523298249846	94.1382547757718982	-32.2316987387113372
p_6	83.7309261448668849	45.3329798362191525	-5.3181367647793465	70.1961989967918498

PARAMETER	VALUE
m_W	80.376 GeV
m_Z	91.1876 GeV
N_f	5
μ	500.0 GeV

$u\bar{d} \to W^+ZZg$	
a_0	-16.6719638614981740
a_{-1}	-22.1957678011010735
a_{-2}	-5.6666666666670213

Table 7. Benchmark point for the subprocess $u(p_1)\bar{d}(p_2) \to W^+(p_3)Z(p_4)Z(p_5)g(p_6)$.

5.6 $pp \to WWW + 1$ jet

Partonic process: $u\bar{d} \to W^+W^-W^+g$.

PARTICLE	E	p_x	p_y	p_z
p_1	250.0000000000000000	0.0000000000000000	0.0000000000000000	250.0000000000000000
p_2	250.0000000000000000	0.0000000000000000	0.0000000000000000	-250.0000000000000000
p_3	89.4258007278425993	27.5517039326065500	-13.1611730250244197	24.5837262194154818
p_4	182.4747913234621421	-128.6494675939613614	-78.7744883983191500	-63.8799073098456347
p_5	141.4314519821789986	54.1746388235997784	97.4403424793774207	-33.3622900835894285
p_6	86.6679559665162316	46.9231248377547274	-5.5046810560337240	72.6584711740195104

PARAMETER	VALUE
m_W	80.376 GeV
m_Z	91.1876 GeV
N_f	5
μ	500.0 GeV

	$u\bar{d} \to W^+W^-W^+g$
a_0	-15.8859769338002099
a_{-1}	-21.9889128719035618
a_{-2}	-5.6666666666864467

Table 8. Benchmark point for the subprocess $u(p_1)\bar{d}(p_2) \to W^+(p_3)W^-(p_4)W^+(p_5)g(p_6)$.

5.7 $pp \to ZZZZ$

Partonic process: $u\bar{u} \to ZZZZ$.

PARTICLE	E	p_x	p_y	p_z
p_1	250.0000000000000000	0.0000000000000000	0.0000000000000000	250.0000000000000000
p_2	250.0000000000000000	0.0000000000000000	0.0000000000000000	-250.0000000000000000
p_3	96.3863867610220666	21.9480082963376795	-10.4843437432888980	19.5836826767025762
p_4	159.2027435644542095	-102.4836644941604078	-62.7526750844588079	-50.8874782857443790
p_5	130.0351856078737001	43.1561483551038094	77.6221118797800074	-26.5767889104262487
p_6	114.3756840666499812	37.3795078427186667	-4.3850930520321931	57.8805845194680018

PARAMETER	VALUE
m_W	80.376 GeV
m_Z	91.1876 GeV
N_f	5
μ	500.0 GeV

	$u\bar{u} \to ZZZZ$
a_0	10.0010268560339206
a_{-1}	-3.9999999999613696
a_{-2}	-2.6666666666665884

Table 9. Benchmark point for the subprocess $u(p_1)\bar{u}(p_2) \to Z(p_3)Z(p_4)Z(p_5)Z(p_6)$.

5.8 $pp \to WWWW$

Partonic process: $u\bar{u} \to W^+W^-W^+W^-$.

PARTICLE	E	p_x	p_y	p_z
p_1	250.0000000000000000	0.0000000000000000	0.0000000000000000	250.0000000000000000
p_2	250.0000000000000000	0.0000000000000000	0.0000000000000000	-250.0000000000000000
p_3	87.7920438094441096	24.8207950462383629	-11.8566452013738353	22.1470015595954024
p_4	168.0494737136866092	-115.8978071108833205	-70.9664068759461202	-57.5481680112689915
p_5	132.1031656516532848	48.8048800986569518	87.7821123452778238	-30.0554392738635485
p_6	112.0553168252159821	42.2721319659877182	-4.9590602679577351	65.4566057255370879

PARAMETER	VALUE
m_W	80.376 GeV
m_Z	91.1876 GeV
N_f	5
μ	500.0 GeV

	$u\bar{u} \to W^+W^-W^+W^-$
a_0	7.8556327396245011
a_{-1}	-3.9999999999981126
a_{-2}	-2.6666666666669747

Table 10. Benchmark point for the subprocess $u(p_1)\bar{u}(p_2) \to W^+(p_3)W^-(p_4)W^+(p_5)W^-(p_6)$.

5.9 $pp \to t\bar{t}b\bar{b}$

Partonic process: $d\bar{d} \to t\bar{t}b\bar{b}$.

PARTICLE	E	p_x	p_y	p_z
p_1	250.0000000000000000	0.0000000000000000	0.0000000000000000	250.0000000000000000
p_2	250.0000000000000000	0.0000000000000000	0.0000000000000000	-250.0000000000000000
p_3	213.1527786548405459	-26.8458616570582116	-117.8628562648380296	-38.8884799556846303
p_4	220.5509350311838546	61.9684848664477599	92.5635212096267281	83.2176445698946168
p_5	42.2714703981682263	-16.8075489037092431	24.9923105627744704	-29.3620149548096769
p_6	24.0248159158073982	-18.3150743056803300	0.3070244924368429	-14.9671496594002438

PARAMETER	VALUE
m_t	171.2 GeV
m_b	4.2 GeV
N_f	4
μ	500.0 GeV

	$d\bar{d} \to t\bar{t}b\bar{b}$
a_0	154.6475673006605973
a_{-1}	2.7409050914577211
a_{-2}	-2.6666666666666683

Table 11. Benchmark point for the subprocess $d(p_1)\bar{d}(p_2) \to t(p_3)\bar{t}(p_4)b(p_5)\bar{b}(p_6)$.

Partonic process: $gg \to t\bar{t}b\bar{b}$.

PARTICLE	E	p_x	p_y	p_z
p_1	250.000000000000000	0.0000000000000000	0.0000000000000000	250.0000000000000000
p_2	250.000000000000000	0.0000000000000000	0.0000000000000000	-250.0000000000000000
p_3	194.0670578462199387	-60.6594324624948058	-47.3641590248774236	-49.2915067154802884
p_4	172.4499944124030151	-15.6689752760792977	-7.1446619651393677	-11.5324581958636152
p_5	61.9093840678718479	12.0715208460656545	23.6785835371366993	55.7560301833003820
p_6	71.5735636735052054	64.2568868925084331	30.8302374528801408	5.0679347280435243

PARAMETER	VALUE
m_t	171.2 GeV
m_b	4.2 GeV
N_f	4
μ	500.0 GeV

	$gg \to t\bar{t}b\bar{b}$
a_0	165.1250038552732349
a_{-1}	-3.4472725930136989
a_{-2}	-6.0000000000001563

Table 12. Benchmark point for the subprocess $g(p_1)g(p_2) \to t(p_3)\bar{t}(p_4)b(p_5)\bar{b}(p_6)$.

5.10 $pp \to t\bar{t} + 2$ jets

Partonic process: $gg \to t\bar{t}gg$. The finite part for this process is given in CDR and was compared with ref. [29].

PARTICLE	E	p_x	p_y	p_z
p_1	2424.7465026975200999	0.0000000000000000	0.0000000000000000	2424.7465026975200999
p_2	2424.7465026975200999	0.0000000000000000	0.0000000000000000	-2424.7465026975200999
p_3	881.9042263139403985	-715.3340594013137661	-475.1625187999429158	101.1925816377931966
p_4	343.4841188963524132	-24.1478321960174789	-6.3283366075706340	295.5085181344487069
p_5	1673.4634600426329598	21.8782679485017297	1000.4115637957629588	1341.3344089052341133
p_6	1950.6412001421140303	717.6036236488295117	-518.9207083882492952	-1738.0355086774759457

PARAMETER	VALUE
m_t	173.3 GeV
N_f	5
μ	173.3 GeV

	$gg \to t\bar{t}gg$	Ref. [29]
a_0	-93.9825428068626394	-93.98254280655584
a_{-1}	47.0991735298819236	47.0991735300671
a_{-2}	-11.9999999999947171	-11.999999999999874

Table 13. Benchmark point for the subprocess $g(p_1)g(p_2) \to t(p_3)\bar{t}(p_4)g(p_5)g(p_6)$.

5.11 $pp \to Z\,b\,\bar{b} + 1$ jet

Partonic process: $ug \to ue^+e^-b\bar{b}$.

PARTICLE	E	p_x	p_y	p_z
p_1	250.0000000000000000	0.0000000000000000	0.0000000000000000	250.0000000000000000
p_2	250.0000000000000000	0.0000000000000000	0.0000000000000000	-250.0000000000000000
p_3	34.5908278264605187	21.2091909896352142	-9.4555401980608202	25.6376353599131122
p_4	166.7223525775519022	-156.7623134542972991	-48.7827423195217946	-29.0200617028515602
p_5	111.6942046513332798	30.9750523871488710	106.1302756897373314	-15.8904394000814051
p_6	84.2714416207739418	35.0918815486497024	1.4231216042880672	76.4890217424595988
p_7	102.7211733238803646	69.4861885288632521	-49.3151147764427051	-57.2161559994397777

PARAMETER	VALUE
m_W	80.376 GeV
w_W	2.124 GeV
m_b	4.2 GeV
N_f	4
μ	500.0 GeV

	$ug \to ue^+e^-b\bar{b}$
a_0	145.3708954680396630
a_{-1}	-8.3679512693708471
a_{-2}	-5.6666666666675392

Table 14. Benchmark point for the subprocess $u(p_1)g(p_2) \to u(p_3)e^+(p_4)e^-(p_5)b(p_6)\bar{b}(p_7)$.

5.12 $pp \to W\,b\,\bar{b} + 1$ jet

Partonic process: $u\bar{d} \to e^+\nu_e b\bar{b}g$.

PARTICLE	E	p_x	p_y	p_z
p_1	250.0000000000000000	0.0000000000000000	0.0000000000000000	250.0000000000000000
p_2	250.0000000000000000	0.0000000000000000	0.0000000000000000	-250.0000000000000000
p_3	93.4300963683620580	-16.6492363753179085	-37.4579803162897420	-83.9576413803095818
p_4	119.9994454272237192	4.7053605726301706	-100.6826015733804809	65.1209660949429150
p_5	57.9859979994296282	9.1381348721238638	-4.6735873988293006	56.9156220722767259
p_6	104.9559149323387999	87.3260122226470514	54.3049824548373437	-20.5728109201014071
p_7	123.6285452726457805	-84.5202712920831658	88.5091868336622554	-17.5061358668087337

PARAMETER	VALUE
m_W	80.376 GeV
w_W	2.124 GeV
m_b	4.2 GeV
N_f	4
μ	500.0 GeV

	$u\bar{d} \to e^+\nu_e b\bar{b}g$
a_0	129.9538554864771243
a_{-1}	-5.3385683701189715
a_{-2}	-5.6666666666668695

Table 15. Benchmark point for the subprocess $u(p_1)\bar{d}(p_2) \to e^+(p_3)\nu_e(p_4)b(p_5)\bar{b}(p_6)g(p_7)$.

5.13 $pp \to W b\bar{b} + 2$ jets

Partonic process: $u\bar{d} \to e^+\nu_e b\bar{b}d\bar{d}$.

PARTICLE	E	p_x	p_y	p_z
p_1	250.0000000000000000	0.0000000000000000	0.0000000000000000	250.0000000000000000
p_2	250.0000000000000000	0.0000000000000000	0.0000000000000000	-250.0000000000000000
p_3	125.6965187314100234	-17.0943040170214537	-113.3597903541534748	51.5456838370753374
p_4	72.1993434263444129	25.0205029393394440	42.4573677065765622	52.7644913865970722
p_5	130.5494441454287085	-59.2470822889473183	116.2307891878907924	-2.3883575291830641
p_6	52.9433261580396106	45.1283306603629413	-14.5296908876010313	-23.1878769876905828
p_7	99.1517346871049057	-5.9484899951818377	-31.1690273964595583	-93.9370730297576273
p_8	19.4596328516722785	12.1410427014482281	0.3703517437466808	15.2031323229588882

PARAMETER	VALUE
m_W	80.376 GeV
w_W	2.124 GeV
m_b	4.2 GeV
N_f	4
μ	500.0 GeV

	$u\bar{d} \to e^+\nu_e b\bar{b}d\bar{d}$
a_0	148.2499564138260837
a_{-1}	-7.7272995122163879
a_{-2}	-5.3333333333331892

Table 16. Benchmark point for the subprocess $u(p_1)\bar{d}(p_2) \to e^+(p_3)\nu_e(p_4)b(p_5)\bar{b}(p_6)d(p_7)\bar{d}(p_8)$.

Partonic process: $u\bar{d} \to e^+\nu_e b\bar{b}s\bar{s}$.

PARTICLE	E	p_x	p_y	p_z
p_1	250.0000000000000000	0.0000000000000000	0.0000000000000000	250.0000000000000000
p_2	250.0000000000000000	0.0000000000000000	0.0000000000000000	-250.0000000000000000
p_3	1.8312125180161738	1.2481975210878733	-0.3016228634824342	-1.3055136470806736
p_4	132.0663362603577298	-16.6607423420677527	94.8432229336175965	-90.3808602603960196
p_5	121.6089450080674226	-63.6699664483805989	-102.6429343577717077	13.4780898076629523
p_6	51.8272368161295987	-33.3143054988286877	-36.6615737768635270	-14.6461098360448521
p_7	124.2305315458477253	116.2047315474863467	-2.8413585495376918	43.8361952698163435
p_8	68.4357378515813224	-3.8079147792972257	47.6042666140377335	49.0181986660422169

PARAMETER	VALUE
m_W	80.376 GeV
w_W	2.124 GeV
m_b	4.2 GeV
N_f	4
μ	500.0 GeV

	$u\bar{d} \to e^+\nu_e b\bar{b}s\bar{s}$
a_0	161.1656361677729592
a_{-1}	-1.3276262260753209
a_{-2}	-5.3333333333332735

Table 17. Benchmark point for the subprocess $u(p_1)\bar{d}(p_2) \to e^+(p_3)\nu_e(p_4)b(p_5)\bar{b}(p_6)s(p_7)\bar{s}(p_8)$.

Partonic process: $u\bar{d} \to e^{+}\nu_{e}b\bar{b}gg$.

PARTICLE	E	p_x	p_y	p_z
p_1	250.0000000000000000	0.0000000000000000	0.0000000000000000	250.0000000000000000
p_2	250.0000000000000000	0.0000000000000000	0.0000000000000000	-250.0000000000000000
p_3	118.4116290336479551	49.7302976872290259	-105.1432905838027665	-22.2058512007951201
p_4	9.9876328289379046	7.4336546931814604	4.5250271451401858	4.9007873616352553
p_5	113.2724870353399353	-8.6682847027615033	110.4231681698792471	23.2614225044082019
p_6	50.3648230617062964	-38.8899369624844553	-31.0689344437605435	-6.4241355543198972
p_7	105.2876197360011901	-28.2113391151385819	10.7916624062129962	100.8620009592996638
p_8	102.6758083043666687	18.8056083999740657	10.4723673063308507	-100.3942240702281055

PARAMETER	VALUE
m_W	80.376 GeV
w_W	2.124 GeV
m_b	4.2 GeV
N_f	4
μ	500.0 GeV

	$u\bar{d} \to e^{+}\nu_{e}b\bar{b}gg$
a_0	64.8935770569783301
a_{-1}	-35.9610562256753425
a_{-2}	-8.6666666666670285

Table 18. Benchmark point for the subprocess $u(p_1)\bar{d}(p_2) \to e^{+}(p_3)\nu_{e}(p_4)b(p_5)\bar{b}(p_6)g(p_7)g(p_8)$.

5.14 $pp \to WWb\bar{b}$

Partonic process: $d\bar{d} \to \nu_{e}e^{+}\bar{\nu}_{\mu}\mu^{-}b\bar{b}$.

PARTICLE	E	p_x	p_y	p_z
p_1	250.0000000000000000	0.0000000000000000	0.0000000000000000	250.0000000000000000
p_2	250.0000000000000000	0.0000000000000000	0.0000000000000000	-250.0000000000000000
p_3	25.6649135887983881	15.7119189648809563	-7.6256852614994211	18.8061776088085644
p_4	154.5064489409292605	-136.9768135536888565	-46.2042967903236104	-54.5413446032057010
p_5	96.1603526761926730	22.3143342117606984	88.8440473781699325	-29.2509685474019605
p_6	61.0731578730670606	23.2528867537403734	2.3717946919774544	56.4234743714476039
p_7	93.6199892430268648	58.9397665353324101	-43.8226058551382351	-57.9028973600646211
p_8	68.9751376779857708	16.7579070879743455	6.4367458368138966	66.4655585304161036

PARAMETER	VALUE
m_W	80.376 GeV
m_Z	91.1876 GeV
m_t	171.2 GeV
m_b	4.2 GeV
N_f	4
μ	500.0 GeV

	$d\bar{d} \to \nu_{e}e^{+}\bar{\nu}_{\mu}\mu^{-}b\bar{b}$
a_0	118.3990066409585751
a_{-1}	8.5574384926230991
a_{-2}	-2.6666666666666492

Table 19. Benchmark point for the subprocess $d(p_1)\bar{d}(p_2) \to \nu_{e}(p_3)e^{+}(p_4)\bar{\nu}_{\mu}(p_5)\mu^{-}(p_6)b(p_7)\bar{b}(p_8)$.

Partonic process: $gg \to \nu_e e^+ \bar{\nu}_\mu \mu^- b\bar{b}$.

PARTICLE	E	p_x	p_y	p_z
p_1	250.0000000000000000	0.0000000000000000	0.0000000000000000	250.0000000000000000
p_2	250.0000000000000000	0.0000000000000000	0.0000000000000000	-250.0000000000000000
p_3	25.6649135887983881	15.7119189648809563	-7.6256852614994211	18.8061776088085644
p_4	154.5064489409292605	-136.9768135536888565	-46.2042967903236104	-54.5413446032057010
p_5	96.1603526761926730	22.3143342117606984	88.8440473781699325	-29.2509685474019605
p_6	61.0731578730670606	23.2528867537403734	2.3717946919774544	56.4234743714476039
p_7	93.6199892430268648	58.9397665353324101	-43.8226058551382351	-57.9028973600646211
p_8	68.9751376779857708	16.7579070879743455	6.4367458368138966	66.4655585304161036

PARAMETER	VALUE
m_W	80.376 GeV
m_Z	91.1876 GeV
m_t	171.2 GeV
m_b	4.2 GeV
N_f	4
μ	500.0 GeV

	$gg \to \nu_e e^+ \bar{\nu}_\mu \mu^- b\bar{b}$
a_0	27.4387494492212056
a_{-1}	-7.9555523940773458
a_{-2}	-5.9999999999999885

Table 20. Benchmark point for the subprocess $g(p_1)g(p_2) \to \nu_e(p_3)e^+(p_4)\bar{\nu}_\mu(p_5)\mu^-(p_6)b(p_7)\bar{b}(p_8)$.

5.15 $pp \to WWb\bar{b}+1$ **jet**

Partonic process: $u\bar{u} \to \nu_e e^+ \bar{\nu}_\mu \mu^- b\bar{b}g$.

PARTICLE	E	p_x	p_y	p_z
p_1	250.0000000000000000	0.0000000000000000	0.0000000000000000	250.0000000000000000
p_2	250.0000000000000000	0.0000000000000000	0.0000000000000000	-250.0000000000000000
p_3	18.1435357791203664	10.6794732394995044	-3.3652659935279523	14.2762644514536543
p_4	132.6867460765342059	-121.1435093670056773	-5.2844663256145745	-53.8711159925087628
p_5	92.9820970636741606	17.2946496492191066	87.0024013115393018	-27.8773677719967203
p_6	46.6813566690488102	14.7875289839330328	9.6031823094958089	43.2233378690595345
p_7	69.5794003816978091	41.1619960772432023	-24.4397402957503331	-50.4943772185567497
p_8	53.6926389028252160	9.1521313351918430	14.4565277002773502	50.8934845655482206
p_9	86.2342251270994211	28.0677300819189206	-77.9726387064195876	23.8497740970007897

PARAMETER	VALUE
m_W	80.376 GeV
m_Z	91.1876 GeV
m_t	171.2 GeV
m_b	0.0 GeV
N_f	5
μ^2	500.0 GeV

	$u\bar{u} \to \nu_e e^+ \bar{\nu}_\mu \mu^- b\bar{b}g$
a_0	-38.5591246673060795
a_{-1}	-32.4828496060584442
a_{-2}	-8.3333333333334405

Table 21. Benchmark point for the subprocess $u(p_1)\bar{u}(p_2) \to \nu_e(p_3)e^+(p_4)\bar{\nu}_\mu(p_5)\mu^-(p_6)b(p_7)\bar{b}(p_8)g(p_9)$.

5.16 $pp \to H + 3$ jets

Partonic process: $gg \to Hggg$.

PARTICLE	E	p_x	p_y	p_z
p_1	250.0000000000000000	0.0000000000000000	0.0000000000000000	250.0000000000000000
p_2	250.0000000000000000	0.0000000000000000	0.0000000000000000	-250.0000000000000000
p_3	144.2726812297522656	26.1871426153409317	-66.9976759414063139	3.8924965402436307
p_4	135.5632052379070274	5.8338195550562180	26.5129120011233681	-132.8172227574218596
p_5	75.6651361325424006	-19.2292152047334604	-65.8505932559228597	31.9241206051040152
p_6	144.4989773997982923	-12.7917469656637373	106.3353571962057913	97.0006056120742102

PARAMETER	VALUE
m_H	125.0 GeV
N_f	5
μ	500.0 GeV

	$gg \to Hggg$
a_0	23.4307927578718953
a_{-1}	-56.3734964424517315
a_{-2}	-15.0000000000008757

Table 22. Benchmark point for the subprocess $g(p_1)g(p_2) \to H(p_3)g(p_4)g(p_5)g(p_6)$.

5.17 $pp \to Z t\bar{t} + 1$ jet

Partonic process: $u\bar{u} \to t\bar{t}e^+e^-g$.

PARTICLE	E	p_x	p_y	p_z
p_1	250.0000000000000000	0.0000000000000000	0.0000000000000000	250.0000000000000000
p_2	250.0000000000000000	0.0000000000000000	0.0000000000000000	-250.0000000000000000
p_3	183.2414081421947287	-30.2337217736484156	32.1314578860740667	48.1815850690226029
p_4	199.0327070603159996	74.5268539046026035	-40.9270527537185629	-55.4554134393922311
p_5	70.1181125436057044	-63.0760999348447697	21.5315800178266556	21.7794946135846281
p_6	20.7607087314536756	-7.2430664321972609	-7.1983324871256098	-18.0756472939650585
p_7	26.8470635224299627	26.0260342360878454	-5.5376526630565506	3.5699810507501222

PARAMETER	VALUE
m_Z	91.1876 GeV
m_t	171.2 GeV
N_f	5
μ	500.0 GeV

	$u\bar{u} \to t\bar{t}e^+e^-g$
a_0	-20.4367763710913373
a_{-1}	-25.9078542815554513
a_{-2}	-5.6666666665792098

Table 23. Benchmark point for the subprocess $u(p_1)\bar{u}(p_2) \to t(p_3)\bar{t}(p_4)e^+(p_5)e^-(p_6)g(p_7)$.

Partonic process: $gg \to t\bar{t}e^+e^-g$.

PARTICLE	E	p_x	p_y	p_z
p_1	250.0000000000000000	0.0000000000000000	0.0000000000000000	250.0000000000000000
p_2	250.0000000000000000	0.0000000000000000	0.0000000000000000	-250.0000000000000000
p_3	174.2203895522303014	-25.0977827305029138	-19.5610151031829993	5.5472629175473589
p_4	186.7123996976260685	-14.0800163072181022	56.3619207264196902	-46.6601246640355427
p_5	60.3016377245591073	38.1795332240129639	22.1553968884492853	41.0822241824339116
p_6	18.6184873501163182	5.2347824612577458	-1.6661313271933778	-17.7895792583830961
p_7	60.1470856754682259	-4.2365166475497116	-57.2901711844925998	17.8202168224373914

PARAMETER	VALUE
m_Z	91.1876 GeV
m_t	171.2 GeV
N_f	5
μ	500.0 GeV

	$gg \to t\bar{t}e^+e^-g$
a_0	9.2826425323344441
a_{-1}	-26.2816094048822784
a_{-2}	-9.0000000000005702

Table 24. Benchmark point for the subprocess $g(p_1)g(p_2) \to t(p_3)\bar{t}(p_4)e^+(p_5)e^-(p_6)g(p_7)$.

5.18 $pp \to Ht\bar{t} + 1$ jet

Partonic process: $gg \to Ht\bar{t}g$.

PARTICLE	E	p_x	p_y	p_z
p_1	250.0000000000000000	0.0000000000000000	0.0000000000000000	250.0000000000000000
p_2	250.0000000000000000	0.0000000000000000	0.0000000000000000	-250.0000000000000000
p_3	126.3747891763443505	6.8355633672742222	-3.2652801590882752	6.0992096455298030
p_4	177.2234233286846745	-31.9178657717747534	-19.5439094615872051	-15.8485716665707326
p_5	174.8995128490773538	13.4406996200208031	24.1748981179500326	-8.2771667589629576
p_6	21.5022746458936318	11.6416027844796517	-1.3657084972745175	18.0265287800038720

PARAMETER	VALUE
m_H	126.0 GeV
m_t	172.5 GeV
N_f	5
μ	500.0 GeV

	$gg \to Ht\bar{t}g$
a_0	-37.1842465451705166
a_{-1}	-35.9217497445515619
a_{-2}	-8.9999999999990887

Table 25. Benchmark point for the subprocess $g(p_1)g(p_2) \to H(p_3)t(p_4)\bar{t}(p_5)g(p_6)$.

5.19 $pp \to H + 3$ jets (VBF)

Partonic process: $uu \to gHuu$ (VBF).

PARTICLE	E	p_x	p_y	p_z
p_1	250.0000000000000000	0.0000000000000000	0.0000000000000000	250.0000000000000000
p_2	250.0000000000000000	0.0000000000000000	0.0000000000000000	-250.0000000000000000
p_3	40.1603071333660182	-14.0012702315405289	0.4395613413056457	37.6380324509251736
p_4	127.7084583092647421	-23.4171446211731009	-10.8486559189339324	4.2888607196847408
p_5	145.0573545181100599	-109.8833468186949176	-94.5094823127907233	5.9366610719649477
p_6	187.0738800392591656	147.3017616714085705	104.9185768904190468	-47.8635542425748710

PARAMETER	VALUE
m_H	125.0 GeV
m_Z	91.1876 GeV
w_Z	2.4952 GeV
N_f	5
μ	500.0 GeV

	$uu \to gHuu$
a_0	-94.6818287259862359
a_{-1}	-40.8904107779583796
a_{-2}	-8.3333333333336821

Table 26. Benchmark point for the subprocess $u(p_1)u(p_2) \to g(p_3)H(p_4)u(p_5)u(p_6)$.

5.20 $pp \to H + 4$ jets (VBF)

Partonic process: $uu \to ggHuu$ (VBF).

PARTICLE	E	p_x	p_y	p_z
p_1	250.0000000000000000	0.0000000000000000	0.0000000000000000	250.0000000000000000
p_2	250.0000000000000000	0.0000000000000000	0.0000000000000000	-250.0000000000000000
p_3	77.8540004794647871	-42.9509851388533761	6.0812524321357140	-64.6488718781321126
p_4	179.6868495846460405	66.2917119993839208	-68.8295351006103004	152.1685510599341171
p_5	140.8511015083574875	-29.7530986170501173	2.6554844463192953	-57.6344889901617350
p_6	81.8035523206006161	2.3404081739038114	78.3533883805051659	-23.3899591949725902
p_7	19.8044961069310155	4.0719635826157594	-18.2605901583498813	-6.4952309966676500

PARAMETER	VALUE
m_H	125.0 GeV
m_Z	91.1876 GeV
w_Z	2.4952 GeV
N_f	5
μ	500.0 GeV

	$uu \to ggHuu$
a_0	-85.2117220498222565
a_{-1}	-54.2263214854450339
a_{-2}	-11.3333333333333464

Table 27. Benchmark point for the subprocess $u(p_1)u(p_2) \to g(p_3)g(p_4)H(p_5)u(p_6)u(p_7)$.

Partonic process: $uu \to u\bar{u}Huu$.

PARTICLE	E	p_x	p_y	p_z
p_1	250.0000000000000000	0.0000000000000000	0.0000000000000000	250.0000000000000000
p_2	250.0000000000000000	0.0000000000000000	0.0000000000000000	-250.0000000000000000
p_3	30.3977507329956786	18.6382269943320686	-8.3093459176077840	22.5298582897146815
p_4	146.5123801227517504	-137.7596903034009301	-42.8693308104768249	-25.5022691658345515
p_5	158.9318930425956466	27.2202771824319179	93.2652344091314376	-13.9642109273819610
p_6	73.9640816926485911	30.8380670569460271	1.2506117519626909	67.2170735086997695
p_7	90.1938944090082799	61.0631190696906998	-43.3371694330094499	-50.2804517051979616

PARAMETER	VALUE
m_H	125.0 GeV
m_Z	91.1876 GeV
w_Z	2.4952 GeV
N_f	5
μ	500.0 GeV

	$uu \to u\bar{u}Huu$
a_0	<u>-36.9909931379802686</u>
a_{-1}	<u>-35.2029797282532968</u>
a_{-2}	<u>-8.0000000000000533</u>

Table 28. Benchmark point for the subprocess $u(p_1)u(p_2) \to u(p_3)\bar{u}(p_4)H(p_5)u(p_6)u(p_7)$.

5.21 $pp \to H + 5$ jets (VBF)

Partonic process: $uu \to gggHuu$ (VBF).

PARTICLE	E	p_x	p_y	p_z
p_1	250.0000000000000000	0.0000000000000000	0.0000000000000000	250.0000000000000000
p_2	250.0000000000000000	0.0000000000000000	0.0000000000000000	-250.0000000000000000
p_3	24.3265597158113103	9.0293044031657743	17.9817135111430346	-13.6715452237514459
p_4	74.2975116145394878	11.5035704263332619	29.2267551012052458	-67.3319009520241991
p_5	97.6019108689663568	-72.1835660496625877	4.7127971252997813	-65.5244636825316746
p_6	136.6365204371290929	23.6483158828115840	-47.1886774719599131	-16.0786999325225715
p_7	120.9034677660200998	23.6253257672831865	-14.6581830826285433	117.6632065216435592
p_8	46.2340295975336915	4.3770495700687935	9.9255948169403965	44.9434032691863266

PARAMETER	VALUE
m_H	125.0 GeV
m_Z	91.1876 GeV
w_Z	2.4952 GeV
N_f	5
μ	500.0 GeV

	$uu \to gggHuu$
a_0	<u>-164.8823178520154897</u>
a_{-1}	<u>-81.4472715794169630</u>
a_{-2}	<u>-14.3333333333333570</u>

Table 29. Benchmark point for the subprocess $u(p_1)u(p_2) \to g(p_3)g(p_4)g(p_5)H(p_6)u(p_7)u(p_8)$.

6 Conclusions

The integrand reduction techniques have changed the way to perform the decomposition of scattering amplitudes in terms of independent integrals. In these approaches, the coefficients which multiply each integral can be completely determined algebraically by relying on the knowledge of the universal structure of the residues of amplitudes at each multiple cuts. The residues are irreducible polynomials in the components of the loop momenta which are not constrained by the on-shell conditions defining the cuts. The coefficients of the master integrals are a subset of the coefficients of the residues.

The generalized unitarity strategy implemented within the integrand decomposition requires to solve a triangular system, where the coefficients of the residues, hence of the master integrals, can be projected out of cuts only after removing the contributions of higher-point residues. By adding one more ingredient to this strategy, namely the Laurent series expansion of the integrand with respect to the unconstrained components of the loop momentum, we improved the system-solving strategy, that became diagonal.

We demonstrated that this novel reduction algorithm, now implemented in the computer code Ninja, and currently interfaced to the GoSam framework, yields a very efficient and accurate evaluation of multi-particle one-loop scattering amplitudes, no matter whether massive particles go around the loop or participate to the scattering as external legs. We used GoSam+Ninja to compute NLO corrections to a set of non-trivial processes involving up to *eight* particles.

The level of automation reached in less than a decade by the evaluation of scattering amplitudes at next-to-leading order has been heavily stimulated by the awareness that the methods for computing the virtual contributions were simply not sufficient, while the techniques for controlling the infrared divergencies and, finally, for performing phase-space integration were already available. Nowadays, the scenario is changed, and one-loop contributions to many multi-particle scattering reactions are waiting to be integrated. We hope that these advancements can stimulate the developments of novel methods for computing cross sections and distributions at next-to-leading-order accuracy for *high-multiplicity* final states.

References

[1] Z. Bern, L.J. Dixon, D.C. Dunbar and D.A. Kosower, *One-loop n-point gauge theory amplitudes, unitarity and collinear limits*, *Nucl. Phys.* **B 425** (1994) 217 [`hep-ph/9403226`] [INSPIRE].

[2] F. Cachazo, P. Svrček and E. Witten, *MHV vertices and tree amplitudes in gauge theory*, *JHEP* **09** (2004) 006 [`hep-th/0403047`] [INSPIRE].

[3] R. Britto, F. Cachazo and B. Feng, *New recursion relations for tree amplitudes of gluons*, *Nucl. Phys.* **B 715** (2005) 499 [`hep-th/0412308`] [INSPIRE].

[4] R. Britto, F. Cachazo and B. Feng, *Generalized unitarity and one-loop amplitudes in $N = 4$ super-Yang-Mills*, *Nucl. Phys.* **B 725** (2005) 275 [`hep-th/0412103`] [INSPIRE].

[5] F. del Aguila and R. Pittau, *Recursive numerical calculus of one-loop tensor integrals*, *JHEP* **07** (2004) 017 [`hep-ph/0404120`] [INSPIRE].

[6] G. Ossola, C.G. Papadopoulos and R. Pittau, *Reducing full one-loop amplitudes to scalar integrals at the integrand level*, *Nucl. Phys.* **B 763** (2007) 147 [`hep-ph/0609007`] [INSPIRE].

[7] C. Berger et al., *An automated implementation of on-shell methods for one-loop amplitudes*, *Phys. Rev.* **D 78** (2008) 036003 [`arXiv:0803.4180`] [INSPIRE].

[8] W. Giele and G. Zanderighi, *On the numerical evaluation of one-loop amplitudes: the gluonic case*, *JHEP* **06** (2008) 038 [`arXiv:0805.2152`] [INSPIRE].

[9] S. Badger, B. Biedermann and P. Uwer, *NGluon: A Package to Calculate One-loop Multi-gluon Amplitudes*, *Comput. Phys. Commun.* **182** (2011) 1674 [`arXiv:1011.2900`] [INSPIRE].

[10] G. Bevilacqua et al., *HELAC-NLO*, *Comput. Phys. Commun.* **184** (2013) 986 [`arXiv:1110.1499`] [INSPIRE].

[11] V. Hirschi et al., *Automation of one-loop QCD corrections*, *JHEP* **05** (2011) 044 [`arXiv:1103.0621`] [INSPIRE].

[12] G. Cullen et al., *Automated One-Loop Calculations with GoSam*, *Eur. Phys. J.* **C 72** (2012) 1889 [`arXiv:1111.2034`] [INSPIRE].

[13] S. Agrawal, T. Hahn and E. Mirabella, *FormCalc 7*, *J. Phys. Conf. Ser.* **368** (2012) 012054 [`arXiv:1112.0124`] [INSPIRE].

[14] F. Cascioli, P. Maierhofer and S. Pozzorini, *Scattering Amplitudes with Open Loops*, *Phys. Rev. Lett.* **108** (2012) 111601 [`arXiv:1111.5206`] [INSPIRE].

[15] S. Actis, A. Denner, L. Hofer, A. Scharf and S. Uccirati, *Recursive generation of one-loop amplitudes in the Standard Model*, *JHEP* **04** (2013) 037 [`arXiv:1211.6316`] [INSPIRE].

[16] S. Badger, B. Biedermann, P. Uwer and V. Yundin, *Numerical evaluation of virtual corrections to multi-jet production in massless QCD*, *Comput. Phys. Commun.* **184** (2013) 1981 [`arXiv:1209.0100`] [INSPIRE].

[17] G. Bevilacqua, M. Czakon, C. Papadopoulos, R. Pittau and M. Worek, *Assault on the NLO Wishlist: pp → ttbb̄*, *JHEP* **09** (2009) 109 [arXiv:0907.4723] [INSPIRE].

[18] A. Lazopoulos, *Multi-gluon one-loop amplitudes numerically*, arXiv:0812.2998 [INSPIRE].

[19] W. Giele, Z. Kunszt and J. Winter, *Efficient Color-Dressed Calculation of Virtual Corrections*, *Nucl. Phys.* **B 840** (2010) 214 [arXiv:0911.1962] [INSPIRE].

[20] A. van Hameren, *Multi-gluon one-loop amplitudes using tensor integrals*, *JHEP* **07** (2009) 088 [arXiv:0905.1005] [INSPIRE].

[21] C. Berger et al., *Precise Predictions for W + 3 Jet Production at Hadron Colliders*, *Phys. Rev. Lett.* **102** (2009) 222001 [arXiv:0902.2760] [INSPIRE].

[22] C. Berger et al., *Next-to-Leading Order QCD Predictions for W + 3-Jet Distributions at Hadron Colliders*, *Phys. Rev.* **D 80** (2009) 074036 [arXiv:0907.1984] [INSPIRE].

[23] R.K. Ellis, K. Melnikov and G. Zanderighi, *Generalized unitarity at work: first NLO QCD results for hadronic W⁺3 jet production*, *JHEP* **04** (2009) 077 [arXiv:0901.4101] [INSPIRE].

[24] R.K. Ellis, K. Melnikov and G. Zanderighi, *W + 3 jet production at the Tevatron*, *Phys. Rev.* **D 80** (2009) 094002 [arXiv:0906.1445] [INSPIRE].

[25] C. Berger et al., *Next-to-Leading Order QCD Predictions for Z, γ* + 3-Jet Distributions at the Tevatron*, *Phys. Rev.* **D 82** (2010) 074002 [arXiv:1004.1659] [INSPIRE].

[26] G. Bevilacqua, M. Czakon, A. van Hameren, C.G. Papadopoulos and M. Worek, *Complete off-shell effects in top quark pair hadroproduction with leptonic decay at next-to-leading order*, *JHEP* **02** (2011) 083 [arXiv:1012.4230] [INSPIRE].

[27] A. Denner, S. Dittmaier, S. Kallweit and S. Pozzorini, *NLO QCD corrections to WWbb production at hadron colliders*, *Phys. Rev. Lett.* **106** (2011) 052001 [arXiv:1012.3975] [INSPIRE].

[28] T. Melia, K. Melnikov, R. Rontsch and G. Zanderighi, *NLO QCD corrections for W⁺W⁻ pair production in association with two jets at hadron colliders*, *Phys. Rev.* **D 83** (2011) 114043 [arXiv:1104.2327] [INSPIRE].

[29] G. Bevilacqua, M. Czakon, C. Papadopoulos and M. Worek, *Hadronic top-quark pair production in association with two jets at Next-to-Leading Order QCD*, *Phys. Rev.* **D 84** (2011) 114017 [arXiv:1108.2851] [INSPIRE].

[30] N. Greiner, A. Guffanti, T. Reiter and J. Reuter, *NLO QCD corrections to the production of two bottom-antibottom pairs at the LHC*, *Phys. Rev. Lett.* **107** (2011) 102002 [arXiv:1105.3624] [INSPIRE].

[31] F. Campanario, C. Englert, M. Rauch and D. Zeppenfeld, *Precise predictions for Wγγ +jet production at hadron colliders*, *Phys. Lett.* **B 704** (2011) 515 [arXiv:1106.4009] [INSPIRE].

[32] A. Denner, S. Dittmaier, S. Kallweit and S. Pozzorini, *NLO QCD corrections to off-shell top-antitop production with leptonic decays at hadron colliders*, *JHEP* **10** (2012) 110 [arXiv:1207.5018] [INSPIRE].

[33] N. Greiner, G. Heinrich, P. Mastrolia, G. Ossola, T. Reiter et al., *NLO QCD corrections to the production of W⁺W⁻ plus two jets at the LHC*, *Phys. Lett.* **B 713** (2012) 277 [arXiv:1202.6004] [INSPIRE].

[34] G. Cullen, N. Greiner and G. Heinrich, *Susy-QCD corrections to neutralino pair production in association with a jet*, *Eur. Phys. J.* **C 73** (2013) 2388 [arXiv:1212.5154] [INSPIRE].

[35] F. Campanario, Q. Li, M. Rauch and M. Spira, *ZZ+jet production via gluon fusion at the LHC*, *JHEP* **06** (2013) 069 [arXiv:1211.5429] [INSPIRE].

[36] G. Bevilacqua and M. Worek, *Constraining BSM Physics at the LHC: Four top final states with NLO accuracy in perturbative QCD*, *JHEP* **07** (2012) 111 [arXiv:1206.3064] [INSPIRE].

[37] T. Gehrmann, N. Greiner and G. Heinrich, *Photon isolation effects at NLO in γγ + jet final states in hadronic collisions*, *JHEP* **06** (2013) 058 [arXiv:1303.0824] [INSPIRE].

[38] F. Campanario, M. Kerner, L.D. Ninh and D. Zeppenfeld, *WZ production in association with two jets at NLO in QCD*, *Phys. Rev. Lett.* **111** (2013) 052003 [arXiv:1305.1623] [INSPIRE].

[39] F. Campanario and M. Kubocz, *Higgs boson production in association with three jets via gluon fusion at the LHC: Gluonic contributions*, *Phys. Rev.* **D 88** (2013) 054021 [arXiv:1306.1830] [INSPIRE].

[40] G. Bevilacqua, M. Czakon, M. Krmer, M. Kubocz and M. Worek, *Quantifying quark mass effects at the LHC: A study of pp → bb̄bb̄ + X at next-to-leading order*, *JHEP* **07** (2013) 095 [arXiv:1304.6860] [INSPIRE].

[41] N. Greiner, G. Heinrich, J. Reichel and J.F. von Soden-Fraunhofen, *NLO QCD Corrections to Diphoton Plus Jet Production through Graviton Exchange*, *JHEP* **11** (2013) 028 [arXiv:1308.2194] [INSPIRE].

[42] H. van Deurzen et al., *NLO QCD corrections to the production of Higgs plus two jets at the LHC*, *Phys. Lett.* **B 721** (2013) 74 [arXiv:1301.0493] [INSPIRE].

[43] T. Gehrmann, N. Greiner and G. Heinrich, *Precise QCD predictions for the production of a photon pair in association with two jets*, *Phys. Rev. Lett.* **111** (2013) 222002 [arXiv:1308.3660] [INSPIRE].

[44] G. Cullen et al., *NLO QCD corrections to Higgs boson production plus three jets in gluon fusion*, *Phys. Rev. Lett.* **111** (2013) 131801 [arXiv:1307.4737] [INSPIRE].

[45] H. van Deurzen et al., *NLO QCD corrections to Higgs boson production in association with a top quark pair and a jet*, *Phys. Rev. Lett.* **111** (2013) 171801 [arXiv:1307.8437] [INSPIRE].

[46] F. Campanario et al., *Electroweak Higgs plus Three Jet Production at NLO QCD*, *Phys. Rev. Lett.* **111** (2013) 211802 [arXiv:1308.2932] [INSPIRE].

[47] F. Campanario, M. Kerner, L.D. Ninh and D. Zeppenfeld, *Next-to-leading order QCD corrections to W⁺W⁺ and W⁻W⁻ production in association with two jets*, arXiv:1311.6738 [INSPIRE].

[48] M.J. Dolan, C. Englert, N. Greiner and M. Spannowsky, *Further on up the road: hhjj production at the LHC*, *Phys. Rev. Lett.* **112** (2014) 101802 [arXiv:1310.1084] [INSPIRE].

[49] S. Badger, A. Guffanti and V. Yundin, *Next-to-leading order QCD corrections to di-photon production in association with up to three jets at the Large Hadron Collider*, arXiv:1312.5927 [INSPIRE].

[50] G. Heinrich, A. Maier, R. Nisius, J. Schlenk and J. Winter, *NLO QCD corrections to WWbb production with leptonic decays in the light of top quark mass and asymmetry measurements*, arXiv:1312.6659 [INSPIRE].

[51] P. Mastrolia, E. Mirabella, G. Ossola and T. Peraro, *Scattering Amplitudes from Multivariate Polynomial Division*, *Phys. Lett.* **B 718** (2012) 173 [arXiv:1205.7087] [INSPIRE].

[52] Y. Zhang, *Integrand-Level Reduction of Loop Amplitudes by Computational Algebraic Geometry Methods*, *JHEP* **09** (2012) 042 [arXiv:1205.5707] [INSPIRE].

[53] P. Mastrolia and G. Ossola, *On the Integrand-Reduction Method for Two-Loop Scattering Amplitudes*, *JHEP* **11** (2011) 014 [arXiv:1107.6041] [INSPIRE].

[54] S. Badger, H. Frellesvig and Y. Zhang, *Hepta-cuts of two-loop scattering amplitudes*, *JHEP* **04** (2012) 055 [arXiv:1202.2019] [INSPIRE].

[55] R.H. Kleiss, I. Malamos, C.G. Papadopoulos and R. Verheyen, *Counting to one: reducibility of one- and two-loop amplitudes at the integrand level*, *JHEP* **12** (2012) 038 [arXiv:1206.4180] [INSPIRE].

[56] S. Badger, H. Frellesvig and Y. Zhang, *An integrand reconstruction method for three-loop amplitudes*, *JHEP* **08** (2012) 065 [arXiv:1207.2976] [INSPIRE].

[57] B. Feng and R. Huang, *The classification of two-loop integrand basis in pure four-dimension*, *JHEP* **02** (2013) 117 [arXiv:1209.3747] [INSPIRE].

[58] P. Mastrolia, E. Mirabella, G. Ossola and T. Peraro, *Integrand-Reduction for Two-Loop Scattering Amplitudes through Multivariate Polynomial Division*, *Phys. Rev.* **D 87** (2013) 085026 [arXiv:1209.4319] [INSPIRE].

[59] R. Huang and Y. Zhang, *On genera of curves from high-loop generalized unitarity cuts*, *JHEP* **04** (2013) 080 [arXiv:1302.1023] [INSPIRE].

[60] P. Mastrolia, E. Mirabella, G. Ossola and T. Peraro, *Multiloop Integrand Reduction for Dimensionally Regulated Amplitudes*, *Phys. Lett.* **B 727** (2013) 532 [arXiv:1307.5832] [INSPIRE].

[61] G. Ossola, C.G. Papadopoulos and R. Pittau, *CutTools: a program implementing the OPP reduction method to compute one-loop amplitudes*, *JHEP* **03** (2008) 042 [arXiv:0711.3596] [INSPIRE].

[62] P. Mastrolia, G. Ossola, T. Reiter and F. Tramontano, *Scattering AMplitudes from Unitarity-based Reduction Algorithm at the Integrand-level*, *JHEP* **08** (2010) 080 [arXiv:1006.0710] [INSPIRE].

[63] G. Ossola, C.G. Papadopoulos and R. Pittau, *Numerical evaluation of six-photon amplitudes*, *JHEP* **07** (2007) 085 [arXiv:0704.1271] [INSPIRE].

[64] P. Mastrolia, G. Ossola, C. Papadopoulos and R. Pittau, *Optimizing the reduction of one-loop amplitudes*, *JHEP* **06** (2008) 030 [arXiv:0803.3964] [INSPIRE].

[65] G. Ossola, C.G. Papadopoulos and R. Pittau, *On the Rational Terms of the one-loop amplitudes*, *JHEP* **05** (2008) 004 [arXiv:0802.1876] [INSPIRE].

[66] P. Draggiotis, M. Garzelli, C. Papadopoulos and R. Pittau, *Feynman Rules for the Rational Part of the QCD 1-loop amplitudes*, *JHEP* **04** (2009) 072 [arXiv:0903.0356] [INSPIRE].

[67] M. Garzelli, I. Malamos and R. Pittau, *Feynman rules for the rational part of the Electroweak 1-loop amplitudes*, *JHEP* **01** (2010) 040 [*Erratum ibid.* **1010** (2010) 097] [arXiv:0910.3130] [INSPIRE].

[68] M. Garzelli, I. Malamos and R. Pittau, *Feynman rules for the rational part of the Electroweak 1-loop amplitudes in the R_ξ gauge and in the Unitary gauge*, *JHEP* **01** (2011) 029 [arXiv:1009.4302] [INSPIRE].

[69] M. Garzelli and I. Malamos, *R2SM: A Package for the analytic computation of the R_2 Rational terms in the Standard Model of the Electroweak interactions*, *Eur. Phys. J.* **C 71** (2011) 1605 [arXiv:1010.1248] [INSPIRE].

[70] H.-S. Shao, Y.-J. Zhang and K.-T. Chao, *Feynman Rules for the Rational Part of the Standard Model One-loop Amplitudes in the 't Hooft-Veltman γ_5 Scheme*, *JHEP* **09** (2011) 048 [arXiv:1106.5030] [INSPIRE].

[71] H.-S. Shao and Y.-J. Zhang, *Feynman Rules for the Rational Part of One-loop QCD Corrections in the MSSM*, *JHEP* **06** (2012) 112 [arXiv:1205.1273] [INSPIRE].

[72] B. Page and R. Pittau, *R_2 vertices for the effective ggH theory*, *JHEP* **09** (2013) 078 [arXiv:1307.6142] [INSPIRE].

[73] R.K. Ellis, W. Giele and Z. Kunszt, *A numerical unitarity formalism for evaluating one-loop amplitudes*, *JHEP* **03** (2008) 003 [arXiv:0708.2398] [INSPIRE].

[74] W.T. Giele, Z. Kunszt and K. Melnikov, *Full one-loop amplitudes from tree amplitudes*, *JHEP* **04** (2008) 049 [arXiv:0801.2237] [INSPIRE].

[75] R.K. Ellis, W.T. Giele, Z. Kunszt and K. Melnikov, *Masses, fermions and generalized D-dimensional unitarity*, *Nucl. Phys.* **B 822** (2009) 270 [arXiv:0806.3467] [INSPIRE].

[76] K. Melnikov and M. Schulze, *NLO QCD corrections to top quark pair production in association with one hard jet at hadron colliders*, *Nucl. Phys.* **B 840** (2010) 129 [arXiv:1004.3284] [INSPIRE].

[77] P. Mastrolia, E. Mirabella, G. Ossola, T. Peraro and H. van Deurzen, *The Integrand Reduction of One- and Two-Loop Scattering Amplitudes*, PoS(LL2012)028 [arXiv:1209.5678] [INSPIRE].

[78] P. Mastrolia, E. Mirabella and T. Peraro, *Integrand reduction of one-loop scattering amplitudes through Laurent series expansion*, *JHEP* **06** (2012) 095 [*Erratum ibid.* **1211** (2012) 128] [arXiv:1203.0291] [INSPIRE].

[79] H. van Deurzen, *Associated Higgs Production at NLO with GoSam*, *Acta Phys. Polon.* **B 44** (2013) 2223 [INSPIRE].

[80] D. Forde, *Direct extraction of one-loop integral coefficients*, *Phys. Rev.* **D 75** (2007) 125019 [arXiv:0704.1835] [INSPIRE].

[81] S. Badger, *Direct extraction of one loop rational terms*, *JHEP* **01** (2009) 049 [arXiv:0806.4600] [INSPIRE].

[82] T. Peraro, Integrand-level Reduction at One and Higher Loops, *Acta Phys. Polon.* **B 44** (2013) 2215.

[83] A. van Hameren, *OneLOop: For the evaluation of one-loop scalar functions*, *Comput. Phys. Commun.* **182** (2011) 2427 [arXiv:1007.4716] [INSPIRE].

[84] A. van Hameren, C. Papadopoulos and R. Pittau, *Automated one-loop calculations: A Proof of concept*, *JHEP* **09** (2009) 106 [arXiv:0903.4665] [INSPIRE].

[85] T. Hahn and M. Pérez-Victoria, *Automatized one loop calculations in four-dimensions and D-dimensions*, *Comput. Phys. Commun.* **118** (1999) 153 [hep-ph/9807565] [INSPIRE].

[86] T. Hahn, *Feynman Diagram Calculations with FeynArts, FormCalc and LoopTools*, PoS(ACAT2010)078 [arXiv:1006.2231] [INSPIRE].

[87] P. Nogueira, *Automatic Feynman graph generation*, *J. Comput. Phys.* **105** (1993) 279 [ɪɴSPIRE].

[88] J. Vermaseren, *New features of FORM*, math-ph/0010025 [ɪɴSPIRE].

[89] T. Reiter, *Optimising Code Generation with haggies*, *Comput. Phys. Commun.* **181** (2010) 1301 [arXiv:0907.3714] [ɪɴSPIRE].

[90] G. Cullen, M. Koch-Janusz and T. Reiter, *Spinney: A Form Library for Helicity Spinors*, *Comput. Phys. Commun.* **182** (2011) 2368 [arXiv:1008.0803] [ɪɴSPIRE].

[91] T. Binoth, J.-P. Guillet, G. Heinrich, E. Pilon and T. Reiter, *Golem95: a numerical program to calculate one-loop tensor integrals with up to six external legs*, *Comput. Phys. Commun.* **180** (2009) 2317 [arXiv:0810.0992] [ɪɴSPIRE].

[92] G. Heinrich, G. Ossola, T. Reiter and F. Tramontano, *Tensorial reconstruction at the integrand level*, *JHEP* **10** (2010) 105 [arXiv:1008.2441] [ɪɴSPIRE].

[93] G. Cullen et al., *Golem95C: A library for one-loop integrals with complex masses*, *Comput. Phys. Commun.* **182** (2011) 2276 [arXiv:1101.5595] [ɪɴSPIRE].

[94] G. van Oldenborgh, *FF: a package to evaluate one loop Feynman diagrams*, *Comput. Phys. Commun.* **66** (1991) 1 [ɪɴSPIRE].

[95] R.K. Ellis and G. Zanderighi, *Scalar one-loop integrals for QCD*, *JHEP* **02** (2008) 002 [arXiv:0712.1851] [ɪɴSPIRE].

[96] J.P. Guillet, G. Heinrich and J. von Soden-Fraunhofen, *Tools for NLO automation: extension of the golem95C integral library*, arXiv:1312.3887 [ɪɴSPIRE].

[97] J. Kuipers, T. Ueda, J. Vermaseren and J. Vollinga, *FORM version 4.0*, *Comput. Phys. Commun.* **184** (2013) 1453 [arXiv:1203.6543] [ɪɴSPIRE].

[98] J. Kuipers, T. Ueda and J. Vermaseren, *Code optimization in FORM*, arXiv:1310.7007 [ɪɴSPIRE].

[99] S. Catani, S. Dittmaier and Z. Trócsányi, *One loop singular behavior of QCD and SUSY QCD amplitudes with massive partons*, *Phys. Lett.* **B 500** (2001) 149 [hep-ph/0011222] [ɪɴSPIRE].